



**TRIBHUVAN UNIVERSITY  
INSTITUTE OF ENGINEERING, PULCHOWK CAMPUS  
DEPARTMENT OF ELECTRICAL ENGINEERING**

**A FINAL YEAR PROJECT REPORT  
ON  
“INDUCTIVE POWER TRANSFER: ELECTRIC SCOOTER BASED DESIGN”**

(Submitted to the Department of Electrical Engineering as partial fulfillment of the requirement for the Bachelor in Electrical Engineering)

(EE755)

**PROJECT MEMBERS**

Abinash Man Karmacharya(074BEL302)

Anjana Shrestha(074BEL304)

Dilip Rana(074BEL312)

Ganesh Rai(074BEL314)

**PROJECT SUPERVISOR**

Assoc. Prof. Dr. Nirmal Paudel  
Department of Electrical Engineering

Baisakh 10, 2079 (April 23, 2022)

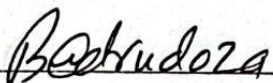


**TRIBHUVAN UNIVERSITY  
INSTITUTE OF ENGINEERING  
PULCHOWK CAMPUS, LALITPUR  
DEPARTMENT OF ELECTRICAL ENGINEERING**

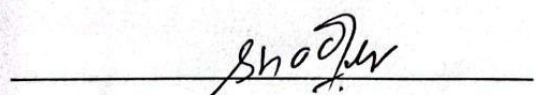
The undersigned certify that they have read and recommended to the Institute of Engineering for acceptance, a project report entitled "**INDUCTIVE POWER TRANSFER: ELECTRIC SCOOTER BASED DESIGN**" submitted by Abinash Man Karmacharya, Anjana Shrestha, Dilip Rana, and Ganesh Rai in partial fulfillment of the requirement for the Bachelor's Degree in Electrical Engineering.

  
Project Supervisor

Associate Prof. Nirmal Paudel, Ph.D.  
Department of Electrical Engineering  
Pulchowk Campus, IOE, TU

  
Head of Department

Associate Prof. Md. Badrudoza  
Department of Electrical Engineering  
Pulchowk Campus, IOE, TU

  
External Examiner

Dr. Shailendra Kr. Jha  
Head of Department of  
Electrical and Electronics Engineering,  
Kathmandu University

## **COPYRIGHT ©**

The author has agreed that the library, Department of Electrical Engineering, Central Campus Pulchowk Campus, Institute of Engineering (IOE) may make this report freely available for inspection. Moreover, the author has agreed that permission for extensive copying of this project report for scholarly purposes may be granted by the supervisor who supervised the project work recorded herein or, in their absence, by the Head of the Department wherein the project report was done. It is understood that recognition will be given to the authors of this report and the Department of Electrical Engineering, Central Campus, Pulchowk, and Institute of Engineering for any use of the material of this project report. Copying or publication or the other use of this report for financial gain without the approval of the Department of Electrical Engineering, Central Campus Pulchowk, Institute of Engineering, and the author's written permission is prohibited. Request for permission to copy or to make any other use of the material in this report in whole or in part should be addressed to:

Head of Department  
Department of Electrical Engineering  
Pulchowk Campus  
Institute of Engineering (IOE)  
Lalitpur, Nepal

## **ACKNOWLEDGEMENT**

Firstly, we would like to express our deep gratitude to our Supervisor **Assoc. Prof. Dr. Nirmal Paudel** for his patience, motivation, and continuous support in our project. We could not have imagined a better advisor and mentor.

We would like to express our due respect to **Assoc. Prof. Mahammed Badrudoza**, Head of the Electrical Engineering Department for his valuable and kind support. Our sincere thanks go to all the professors and lecturers of the department for their precious suggestions and kind support throughout the project duration.

We extend our special thanks to all the **department staff, Madhusudan sir**, and our **friends and families** for their endless support.

And lastly, we express our gratitude to **Ebolt Mobility** for their logistical help and this opportunity to work on this project.

## **Project Members**

**Abinash Man Karmacharya(074BEL302)**

**Anjana Shrestha(074BEL304)**

**Dilip Rana(074BEL312)**

**Ganesh Rai(074BEL314)**

## **ABSTRACT**

Wireless Power Transmission (WPT) system consists of power transmitted between the transmitter and the receiver of the system without any conducting medium between them. Power may be transmitted in the form of an electric field or magnetic field or a combination of both i.e. electromagnetic field. In terms of power transmission capabilities, power transfer efficiency, safety, and ease of control, Tesla's approach based on magnetic resonance coupling surpasses any other techniques. Magnetic resonance or resonant WPT is an improvement in Inductive Power Transfer (IPT) in which the electrical system is forced into resonance. The development of power electronics and the availability of Litz wire revived the magnetic resonance WPT from being limited to studies and research and brought it into applications in the field of portable electronics and medical equipment. Due to high power transfer capability and robustness against misalignment, magnetic resonant WPT has been deemed suitable for charging electric vehicles as well. As our final year project, we sought to develop a wireless charger for an electric scooter based on magnetic resonant WPT to transfer 1kW power up to a distance of 20cm. The project was carried out first in simulation (MATLAB & COMSOL) and then proceeded with hardware implementation right from the scratch. The system was designed to transmit power at a frequency of 85kHz referring to various available standards. Due to the unavailability of components and cost limitations, the amount of power transferred had to be reduced to 100W. Maximum efficiency of 94.9% was achieved for the transfer of 110W at a distance of 10cm and 92 kHz frequency. In this report, we have aspired to encompass the findings of building such a wireless charger for an electric scooter.

## TABLE OF CONTENTS

<b>COPYRIGHT ©</b>	<b>ii</b>
<b>ACKNOWLEDGEMENT</b>	<b>iii</b>
<b>ABSTRACT</b>	<b>iv</b>
<b>TABLE OF CONTENTS</b>	<b>v</b>
<b>LIST OF FIGURES</b>	<b>vii</b>
<b>LIST OF ABBREVIATIONS</b>	<b>ix</b>
<b>CHAPTER ONE</b>	<b>1</b>
<b>INTRODUCTION</b>	<b>1</b>
1.1 Background	1
1.2 Problem Statement	3
1.3 Objective	4
1.4 Scope of the Project	4
1.5 Project Layout	4
<b>CHAPTER TWO</b>	<b>5</b>
<b>RELATED THEORIES</b>	<b>5</b>
2.1 Inductive Power Transfer (IPT)	5
2.2 Magnetic Resonance IPT	7
2.3 Equivalent Circuits of the Coupled Inductors	8
2.4 Skin Effect and Proximity Effect	10
2.5 Coil Design	11
2.6 Compensation Networks	12
2.7 Half-Bridge Inverter	14
<b>CHAPTER THREE</b>	<b>16</b>
<b>LITERATURE REVIEW</b>	<b>16</b>
<b>CHAPTER FOUR</b>	<b>18</b>
<b>METHODOLOGY</b>	<b>18</b>
4.1 Software Simulation	18
4.1.1 Selection and Design of Coil	18
4.1.1.1 Core Selection	19
4.1.1.2 Conductor Selection	19
4.1.1.3 Coil Design	20
4.1.2 Design of Circuits	21
4.1.2.1 Harmonic Inhibitor Block	22
4.1.2.2 Inverter Block	24

4.1.2.3 Coil Block	24
4.1.2.4 Receiver Block	25
4.1.3 Simulation Results	27
4.1.4 Redesign Due to Hardware Limitations	28
4.1.4.1 Elimination of harmonic inhibitor circuit	29
4.1.4.2 Elimination of shielding core	29
4.1.4.3 Change of Coil Design	29
4.1.4.4 Change in compensation topology	31
4.1.4.1 Change in DC Output of AC to DC converter	31
4.1.4.1 Elimination of Voltage Regulation in the Receiver Circuit	31
4.2 Hardware Implementation	32
4.2.1 Transmitter Coil	32
4.2.2 Receiver Coil	33
4.2.3 Transmitter Compensation Capacitor	33
4.2.4 Receiver Compensation Capacitor	34
4.2.5 Power Supply (Inverter)	34
4.2.6 Rectifier with Filter	35
4.2.7 Inverter (Half-bridge)	36
4.2.8 Gate Driver	38
4.2.9 Oscillator	39
4.2.10 Voltage Controlled Oscillator	40
4.2.11 Output Rectifier and Voltage Regulator	41
<b>CHAPTER FIVE</b>	<b>42</b>
<b>RESULTS AND DISCUSSION</b>	<b>42</b>
5.1 Observation of Waveforms	42
5.1.1 Gate Driving Transformer Outputs	42
5.1.2 Output of the Inverter	43
5.1.3 Receiver Output	43
5.1.4 Receiver Output when using LED Lights as the Load	44
5.2 Collection and Interpretation of the Data	44
5.2.1 $P_{out}$ vs f and $V_{out}$ vs f for $RL = 20/6$ Ohm at Different Distances	45
5.2.2 $P_{out}$ vs f and $V_{out}$ vs f for $RL = 20/4$ Ohm at Different Distances	46
5.2.3 $P_{out}$ vs f and $V_{out}$ vs f for $RL = 20/2$ Ohm at Different Distances	47
5.2.4 Max Efficiency vs Load for the Open Circuit at Different Distances	48
<b>CHAPTER SIX</b>	<b>49</b>
<b>CONCLUSION AND RECOMMENDATION</b>	<b>49</b>
<b>REFERENCES</b>	<b>50</b>

## LIST OF FIGURES

Fig 1.1: Various Types Of Wireless Power Transfer Mechanisms[4]	2
Fig 1.2: The Deployed Tx Coil Of The Stationary Charging System At Bus Stops, Deployed In Waseda University, Japan[5]	2
Fig 1.3: Generic Structure Of A Wireless Ev Charger[2]	3
Fig 2.1: Ampere's Law (Right-Hand Screw Rule)	5
Fig 2.2: Faraday's Law	6
Fig 2.3: Equivalent Circuit of IPT	7
Fig 2.4: Inductive Power Transfer with a Compensation Network	7
Fig 2.5: Variation of Efficiency and Receiving End Power with Distance[4]	8
Fig 2.6: Equivalent Circuit [4]	8
Fig 2.7: T-Model Equivalent Circuit[4]	9
Fig 2.8: Comparison of Current through a Solid Conductor and Litz Wire[4]	11
Fig 2.9: Four Different Coil Topologies and the Respective Output Power Variation with the Position[5]	12
Fig 2.10: a) Series-Series (S-S) Compensation, b)Series-Parallel (S-P) Compensation, c) Parallel-Series (P-C) Compensation, d) Parallel-Parallel (P-P) Compensation[2]	13
Fig 2.11: LCL Compensation Network Topology	13
Fig 2.12: LCC Compensation Network Topology	14
Fig 2.13: Half-Bridge Inverter [6]	14
Fig 2.14: Waveforms of the Output Voltage of the Half-Bridge Inverter[7]	15
Fig 2.15: Half-Bridge Inverter Implemented with IGBT[8]	15
Fig 4.1: Distribution of Current Density in (a) Copper Cable, and (b) Litz Wire[2]	20
Fig 4.2: Selected Coil Design	21
Fig 4.3: Schematic Diagram of the System	22
Fig 4.4: Harmonic Inhibitor Circuit	23
Fig 4.5: Inverter Circuit Diagram	24
Fig 4.6: Schematic Diagram of Coil Block	25
Fig 4.7: Schematic Diagram of Receiver Circuit	26
Fig 4.8: Input Current and Voltage Waveforms	27
Fig 4.9: Output Current and Voltage	27
Fig 4.10: Schematic Diagram of the Redesigned System	28
Fig 4.11: Magnetic Field Contour Plot without Core (Left), and with Core (Right)	29
Fig 4.12: Cost Comparison of Different Coil Designs	30
Fig 4.13: Schematic Diagram of Coil Block for New Design	31
Fig 4.14: Transmitter Coil	32
Fig 4.15: Receiver Coil	33
Fig 4.16: Transmitter Compensation Capacitor	33
Fig 4.17: Receiver Compensation Capacitor	34

Fig 4.18: Rectifier with Capacitor Hardware	35
Fig 4.19: Rectifier with Capacitor Schematic	35
Fig 4.20: Inverter Hardware	36
Fig 4.21: Inverter Schematic	36
Fig 4.22: Gate Driver Hardware	38
Fig 4.23: Gate Driver Schematic	38
Fig 4.24: Oscillator Hardware	39
Fig 4.25: Oscillator Schematic	39
Fig 4.26: Voltage Controlled Oscillator Hardware	40
Fig 4.27: Voltage Controlled Oscillator Schematic	40
Fig 4.28: Output Rectifier and Voltage Regulator Hardware	41
Fig 5.1: The Output of the Gate Driving Circuit	42
Fig 5.2: Inverter Output Signal	43
Fig 5.3: Output Signal at Receiver Side with Resistive Load	43
Fig 5.4: Output Signal at Receiver Side with LED Load	44
Fig 5.5: $P_{out}$ vs f at 20/6 Ohm	45
Fig 5.6: $V_{out}$ vs f at 20/6 Ohm	45
Fig 5.7: $P_{out}$ vs f at 20/4 Ohm	46
Fig 5.8: $V_{out}$ vs f at 20/4 Ohm	46
Fig 5.9: $P_{out}$ vs f at 20/2 Ohm	47
Fig 5.10: $V_{out}$ vs f at 20/2 Ohm	47
Fig 5.11: Max Efficiency vs Load	48

## **LIST OF ABBREVIATIONS**

AC	- Alternating Current
AWG	- American Wire Gauge
CPT	- Capacitive Power Transfer
DC	- Direct Current
EMF	- Electromotive Force
EV	- Electric Vehicle
IMD	- Implantable Medical Devices
IPT	- Inductive Power Transfer
LPT	- Laser Power Transfer
MOSFET	- Metal Oxide Field Effect Transistor
MPT	- Microwave Power Transfer
Op-Amp	- Operational Amplifier
P-P	- Parallel-Parallel Compensation
P-S	- Parallel-Series Compensation
S-P	- Series-Parallel Compensation
SPS	- Solar Power Satellites
S-S	- Series- Series Compensation
WPT	- Wireless Power Transfer

# CHAPTER ONE

## INTRODUCTION

### 1.1 Background

Wireless power transfer, wireless power transmission, wireless energy transmission, or electromagnetic power transfer is the transmission of electrical energy without wires as a physical link.<sup>[1]</sup> Nikola Tesla conducted the first wireless power transfer experiments near the end of the nineteenth century. He was able to transmit power between two objects 48 kilometers apart using microwaves. Another of Tesla's trials involved powering 200 lamps without cords from a 25-mile-away power source.<sup>[2]</sup> M. Hulin and M. LeBlanc suggested the equipment and a method for inductively powering an electrical vehicle (EV) utilizing an alternating current (AC) generator of around 3-kHz frequency around the same time, in 1894. Electric vehicles (EVs) were invented over 100 years ago, shortly after the steam engine. The EV, however, went out of popularity with the introduction of the internal combustion engine. As a result, the EV inductive-coupling WPT charger was forgotten after Hulin and LeBlanc, just as Tesla's WPT dream was forgotten after him.<sup>[3]</sup>

Wireless Power Transfer (WPT) systems did not resurface in the research community until the twenty-first century. The invention of power converters at that time fueled this fresh enthusiasm, allowing for frequency ranges of dozens of kHz and kW operations, previously impossible. The technology was initially referred to as contactless Energy Transfer in this new trend (CET). However, the term "wireless power transfer" eventually came to be adopted.<sup>[2]</sup> H. Yagi and S. Uda from Japan and H. V. Noble from the United States demonstrated wireless power transfer using high-frequency microwaves. We now have the same WPT dream as Tesla, Hulin, and LeBlanc did a century ago. There have been several studies, advances, and commercial products based on WPT technology throughout the last century.<sup>[3]</sup>

WPT technology has now become a reality found in commercial devices such as electric toothbrushes, mobile phone power mats, and even electric vehicle chargers (EVs). In 2017, 450 million items with this functionality were shipped around the world, mostly in smartphones, smartwatches, and small household appliances. This statistic marked a 75 percent increase over the previous year's sales. Soon, this large increase is projected to continue.

Due to its advantages of being cordless, safe when charging, and the ability to work in a damp and hostile environment, WPT is a promising technology. This is now being employed in a variety of applications, including electric vehicles (EVs), superconducting magnetic levitation trains (maglev), implantable medical devices (IMDs), and consumer electronics. The WPT technology can be split into two groups based on the energy transfer method: Near field(Inductive power transfer (IPT), capacitive power transfer (CPT)) and far-field (microwave power transfer (MPT), laser power transfer (LPT), and solar power satellites (SPS). Due to its importance and rapid development, WPT has been widely used over the last few years, offering a practical technique to transfer power wirelessly in many applications on a commercial scale.

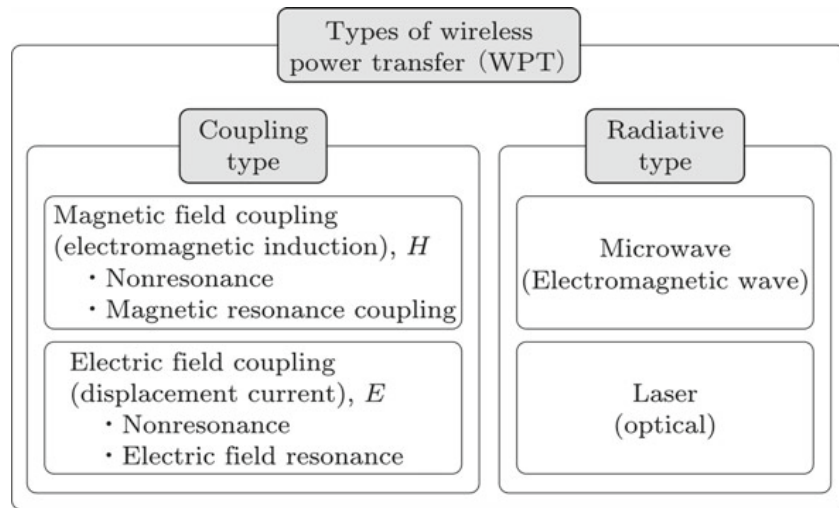


**Fig 1.1: Various Types of Wireless Power Transfer Mechanisms<sup>[4]</sup>**

Magnetic resonance or resonant WPT is an improvement on inductive WPT, electrical systems are forced to work under resonant conditions. The pair of coils is connected to structures composed of reactive elements such as capacitors or additional coils referred to as compensation networks. The technology uses the electromagnetic induction phenomenon and accomplishes wireless power transfer with a circuit topology consisting of resonant circuits on both sides.

The availability of Litz wire during the 1950s helped to maintain low resistance at high frequencies and increase flexibility, and the development of high-frequency power electronics devices opened the gateway for diverse applications of WPT and EVs have not been able to remain indifferent. At present, many universities, manufacturers, and research companies have invested their time and resources to develop high-efficiency wireless charging systems.



**Fig 1.2: The Deployed Tx Coil of the Stationary Charging System at Bus Stops, Deployed in Waseda University, Japan<sup>[5]</sup>**

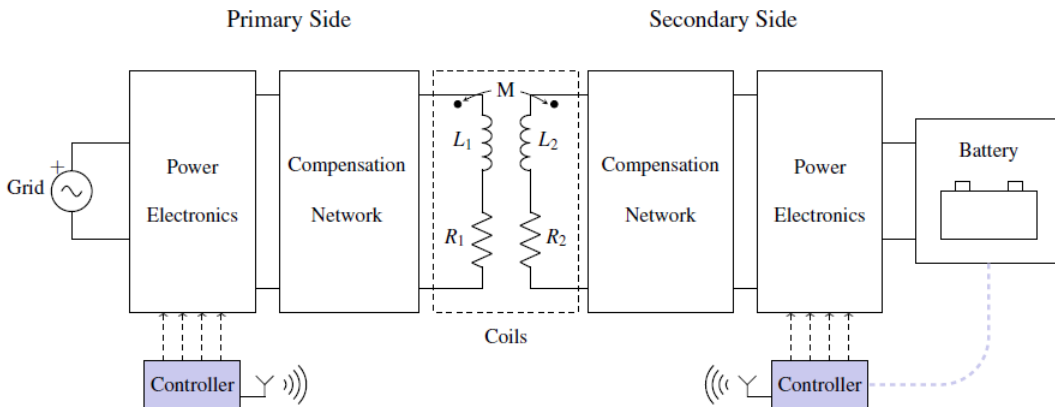


**Fig 1.3: Generic Structure of a Wireless EV Charger<sup>[2]</sup>**

The wireless charger's structure is divided into two parts: the primary and secondary sides as shown in the figure above. The pieces that connect the utility grid to the coil embedded in the pavement make up the primary side. The vehicle's components are connected to the secondary side. This type of wireless charger is made up of two pairs of coils. The primary/transmitter coil and the secondary/receiver/pick-up coil are the two coils. The primary coil is energized with a time-varying current using magnetic resonance technology. A magnetic field is created as a result. A voltage is induced in the secondary coil's terminals when the magnetic field passes through it. The system is operated in resonance to maximize its efficiency.

The utility grid supply frequency is insufficient to achieve a reasonable rate of magnetic flux change, hence power converters are also required. On the primary side, the power converter raises the grid's frequency, while on the secondary side, the power converter converts the AC signal sent between the coils into a DC signal suitable for charging the vehicle's battery. The frequency of the magnetic field used in this WPT is normally in the range of hundreds. Power electronics circuits are useful to control the output voltage and current at the receiver side according to the battery requirements with the help of a controller. Such a charger may have unidirectional or bidirectional power flow depending upon the design.

## 1.2 Problem Statement

As the journey to make the world a greener place is progressing, Electric Vehicles(EVs) are receiving greater acceptance. In countries like Nepal, taxes on EVs have been reduced to almost 1/4th and electricity availability has improved. With present charging technologies, there could be a lot of hassle, chances of electrocution, and mechanical damage due to wear and tear in daily charging of electric vehicles in daily use cases. Hence, a convenient and practicable system must be developed, so that the charging of vehicles becomes hassle-free and efficient. Apart from that, such charging activities introduce a lot of harmonics in the source with the additional disadvantage of poor power factor.

Despite the electric and environmental benefits of EVs, drivers are still hesitant to

utilize them because they feel they will limit their autonomy. As a result, new convenient and user-friendly ways are required to encourage the greater usage of electric vehicles. WPT is a potential technology for this mode of transportation in this context.

### **1.3 Objective**

The main objective of this project is:

- To transfer the power wirelessly over a distance of approximately 20 cm using inductive resonance coupling with and reduce its effect on the source
- To facilitate the easy charging of electric scooters which are generally placed in the same location at home, workplace, etc.

### **1.4 Scope of the Project**

The scope of this project includes:

- 1) User convenience and hassle-free charging of electric scooters.
- 2) No mechanical wear and tear due to rapid plugging and unplugging.
- 3) Safety for human beings.
- 4) Efficient and noiseless.
- 5) Less chance of electrical failure due to exposed sockets.

### **1.5 Project Layout**

This project consists of five chapters including the current chapter. This chapter – Introduction includes the theoretical background, problem statement, objectives, and scope of this project.

Chapter two provides a literature review on theoretical articles or publications from conferences or transactions as well as books from major publishers. The available information and previous results from other research related to the design and fabrication of magnetic resonance coupled inductive power transfer arrangements are summarized in this section.

Chapter three includes the proposed layout of the project and the methods and tools that were implemented to attain the objectives of the project.

Chapter four presents the results that have been obtained during the implementation of this project. Also, the discussion on the obtained results is performed.

Chapter five gives conclusions about this project and suggestions for future work.

## CHAPTER TWO

### RELATED THEORIES

In this chapter, we discuss the inductive power transfer (IPT), magnetic resonance IPT, the equivalent circuit of coupled inductors, skin effect and proximity effect, coil design, compensation networks, and half-bridge inverter, which are the vital theories forming the foundation of the entire project.

#### 2.1 Inductive Power Transfer (IPT)

Inductive Power Transfer (IPT) is a type of near-field power transfer characterized by the use of a magnetic field to transfer power. The interaction of magnetic and electrical behavior described by Ampère's Law and Faraday's Law explains the operation concept, both of which are also a part of Maxwell's equations. According to Ampere's Law, a current-carrying wire establishes a magnetic field in its vicinity. The topology of the wire determines the magnetic field's intensity and orientation. Ampère's Law can be stated mathematically as:

$$\oint \overline{H} dl = I \quad (2.1)$$

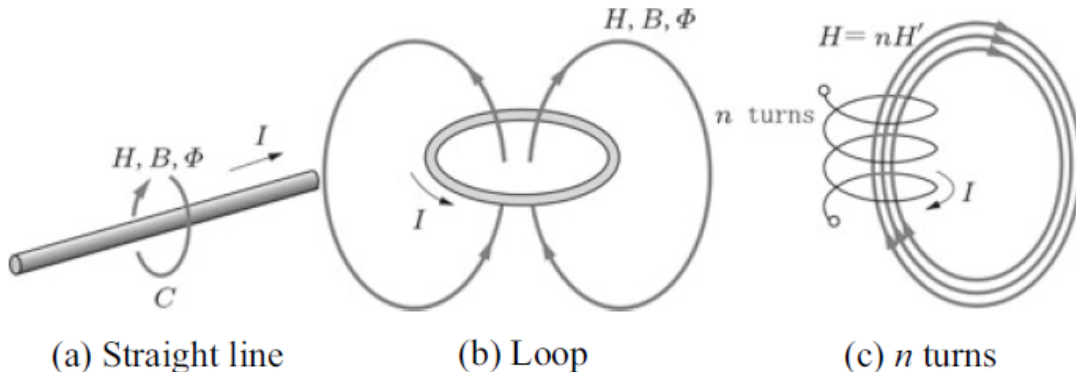


**Fig 2.1: Ampere's Law (Right-Hand Screw Rule)**

where  $\overline{H}$  denotes the magnetic field intensity of the magnetic field generated by the electric current  $I$  and  $dl$  is the infinitesimally small length taken along the current path. The frequency at which the magnetic field's intensity varies is equal to the frequency of the wire's current. The magnetic field can be concentrated using more turns.

When the four fingers of our right hand are curled along the direction of the current, then the thumb gives the direction of the magnetic field. This is called the right-hand screw rule. Similarly, if the thumb represents the current direction, then the curl of our fingers indicates the direction of magnetic flux around the conductor. This is called the right-hand thumb rule.

Thus, from Ampere's law, alternating current through the coil produces an alternating magnetic field around the coil whose distribution depends on the coil topology. When that time-varying magnetic field passes through a separate coil, it induces a voltage ( $e_{ind}$ ) in its terminals. The magnitude of electromotive force induced across the other coil is given by:

$$e_{ind} = - \frac{d\Phi}{dt} \quad (2.2)$$

where  $\Phi$  represents the magnetic field passing through the coil.

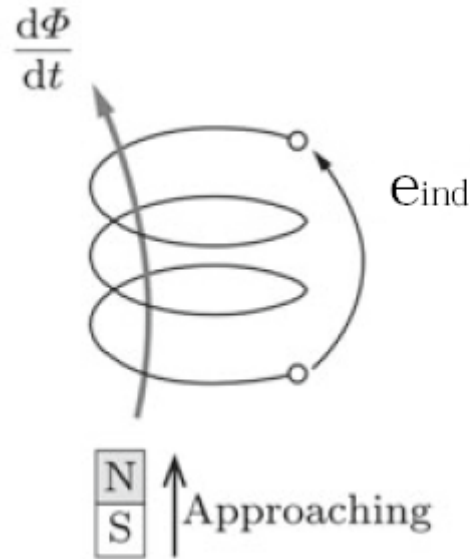


**Fig 2.2: Faraday's Law**

These two phenomena are the basis for inductive and other magnetic-based WPT technologies. Two coils, namely transmitting (primary) and receiving (secondary) coils are required to carry out Inductive WPT. The primary side is supplied with the time-varying source and the resulting magnetic field must traverse the receiving coil. The secondary side is connected to the load directly or through some electronic circuits.

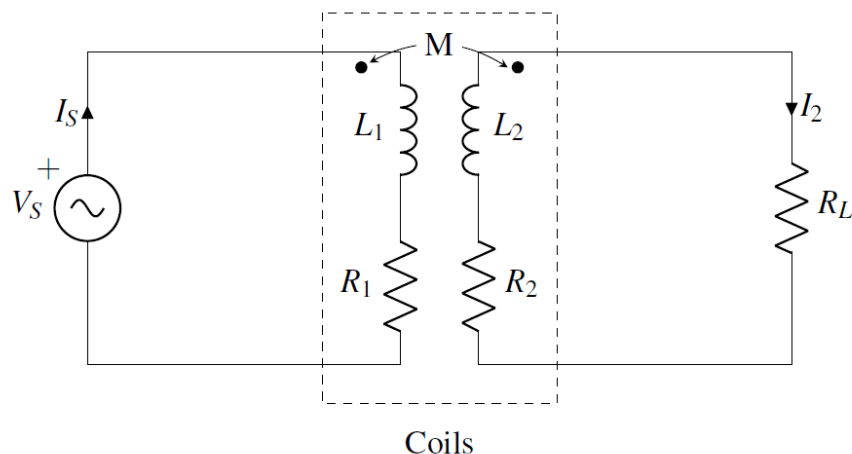


**Fig 2.3: Equivalent Circuit of IPT**

As per Faraday's law of electromagnetic inductions, the voltage induced is directly proportional to the rate of change of magnetic flux. As mentioned above, the rate of change of flux depends on the frequency of current through the coil, the emf induced therefore depends upon the frequency of the source. Therefore, a higher frequency is required to induce a higher voltage in the secondary circuit. Apart from that, it is required that most of the field generated by the sending side passes through the receiver side. For this purpose, bigger coils are used which is limited by the housing of such coils. However, high frequency using advanced power electronics is highly supported by EVs.<sup>[2]</sup>

## 2.2 Magnetic Resonance IPT

Magnetic resonance or resonant WPT, in which the electrical system is made to work under resonant conditions, can be regarded as an improvement on Inductive WPT. The pair of coils is coupled to reactive elements, such as capacitors or extra coils. These structures are known as compensation networks.

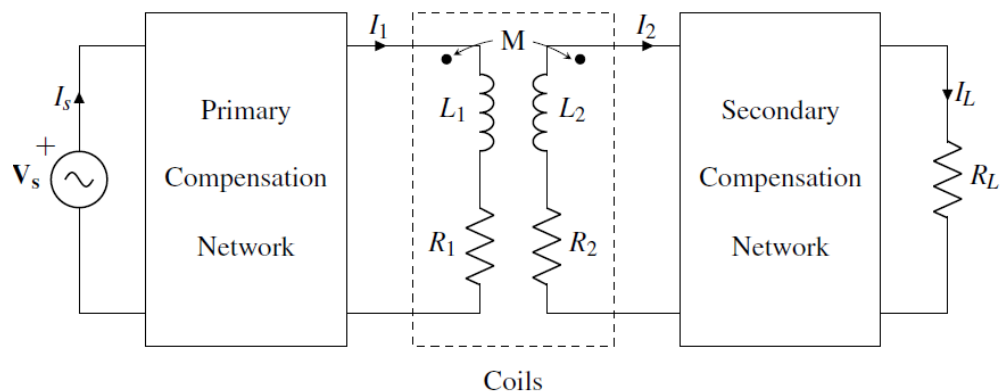


**Fig 2.4: Inductive Power Transfer with a Compensation Network**

The most basic compensation topologies consist of a single capacitor connected in series or parallel to the main and secondary coils. These networks are known as mono-resonant compensation topologies. More complex compensation topologies exist as well, known as multi-resonant compensation topologies. Wireless EV chargers are implemented using compensation networks.<sup>[2]</sup> The line between electromagnetic induction and magnetic resonant coupling is drawn only by operation under resonance conditions. Operation in resonance conditions increases both efficiency and power through the air gap.<sup>[4]</sup>

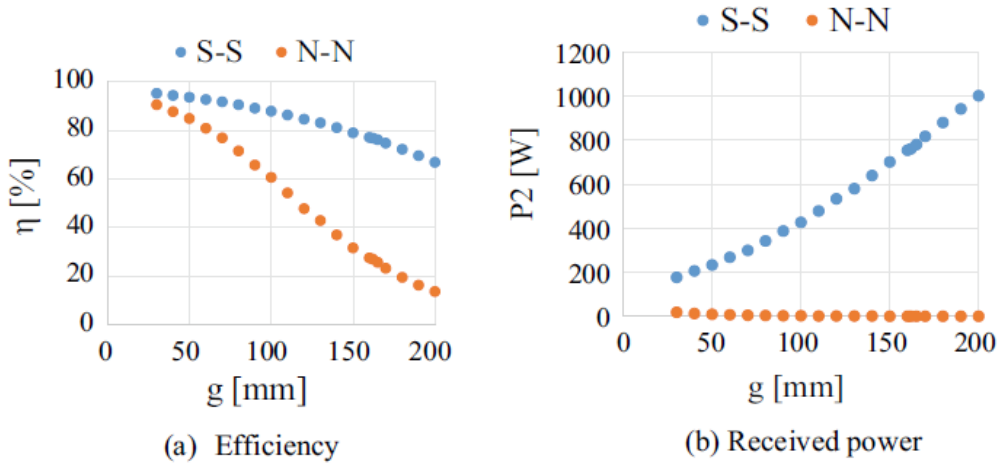


**Fig 2.5: Variation of Efficiency and Receiving End Power with Distance<sup>[4]</sup>**

As the distance between the receiver and transmitter increases, the amount of power also decreases which resonance condition operation compensates. Thus, resonance helps to overcome the distance limitation of such near-field transfer.

### 2.3 Equivalent Circuits of the Coupled Inductors

A pair of coupled inductors is exactly similar to a transformer having an air core. However, the coupling coefficient  $k$  is nearly unity in the case of transformers whereas the values are much smaller in the case of coils for wireless power transmission.

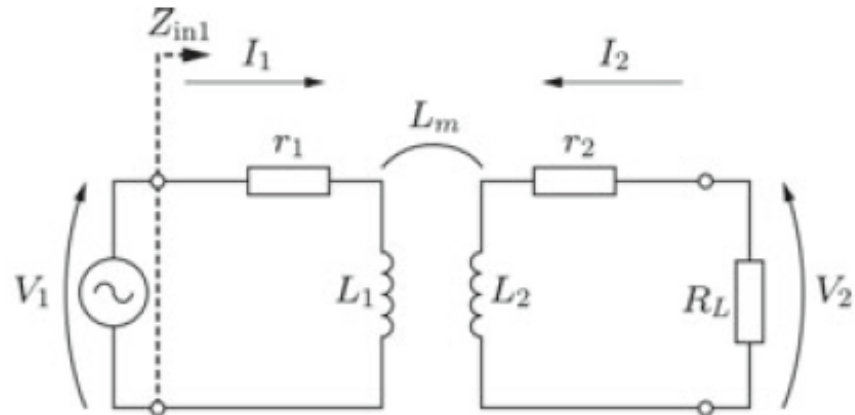


**Fig 2.6: Equivalent Circuit<sup>[4]</sup>**

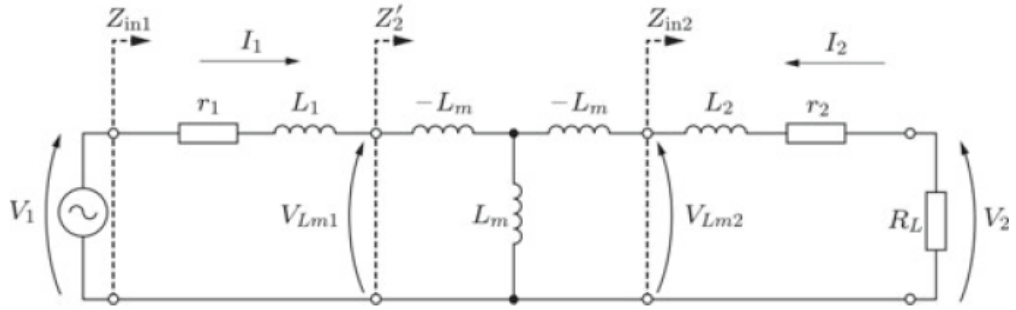


**Fig 2.7: T-Model Equivalent Circuit<sup>[4]</sup>**

As the primary side is connected to the source, current flows and produces an alternating magnetic field as per Ampere's law. A portion of magnetic flux links with the secondary side whereas the remaining part links with itself. The secondary side produces magnetic flux in the direction that cancels the magnetic flux. Voltage  $V_{Lm2}$  is the voltage induced at the secondary side due to the current  $I_1$  flowing in the primary.

$$V_{Lm2} = j\omega L_m I_1 \quad (2.3)$$

On the other hand, the voltage in the secondary causes the current  $I_2$  in the circuit. This causes a voltage drop in the primary side which is given by:

$$V_{Lm1} = j\omega L_m I_2 \quad (2.4)$$

In the figure above  $Z_{in1}$ ,  $Z'_2$ , and  $Z_{in2}$  represent impedance seen from the respective points seen from that particular point. Moreover, these are termed the reflected impedance. The voltage  $V_{Lm1}$  when divided by the current  $I_1$  gives  $Z'_2$  which is the secondary side impedance on the primary side.

$$Z'_2 = \frac{V_{Lm1}}{I_1} = \frac{j\omega L_m I_2}{I_1} = \frac{(j\omega L_m)^2}{Z_{in2}} \quad (2.5)$$

Here,  $L_m$  represents the portion of total inductance in the primary side whose voltage drop is linked to the secondary side.  $L_m$  depends upon the value of the coupling coefficient and the values of the primary and secondary self-inductances. If  $L_1$  and  $L_2$  are the primary sides and secondary side inductances respectively, then the value of the coupling coefficient is given by:

$$k = \frac{L_m}{\sqrt{L_1 L_2}} \quad (2.6)$$

$$k = \frac{L_m}{L} \quad (2.7)$$

where  $L$  represents the geometric mean of the inductances of the transmitting and the receiving coils. Values of  $k$  range between 0 and 1. If  $k = 0$ , then there is no coupling between the coils. But if  $k = 1$ , the coils are said to be fully coupled and all the flux produced by the primary coil passes through the secondary coil. In the case of IPT, the value of the coupling coefficient is always less than 1.

As the distance between the coils increases, the value of the coupling coefficient decreases. The value of mutual inductance decreases and the voltage drop on it decreases as well. Therefore, the voltage appearing on the secondary side decreases as well reducing the power transfer.

## 2.4 Skin Effect and Proximity Effect

If the current passing through the conductor is alternating, the effective resistance offered by the conductor is different from the DC resistance of the conductor. This is due to the skin effect and proximity effect. Skin effect is the resistance produced by the conductor in itself when a high-frequency current flows through it. The proximity effect is caused due to the two wires carrying high-frequency current in the vicinity of each other. Skin depth is defined as the depth from the surface with a flowing current. It is expressed as:

$$\delta = \sqrt{\frac{2}{\omega \sigma \mu}} \quad (2.8)$$

Then, the effective resistance for a circular wire considering skin effect is given by:

$$R_{ohm} = \frac{\rho l}{\pi \rho (D - \delta)} \quad (2.9)$$

Skin effect and proximity effect are caused due to variation of magnetic flux linkage along the cross-section of the conductor. To overcome both the skin effect and the proximity effect, instead of using a solid conductor, multiple small conductors are stranded together to form a composite conductor. Such stranded conductors are called Litz wire.

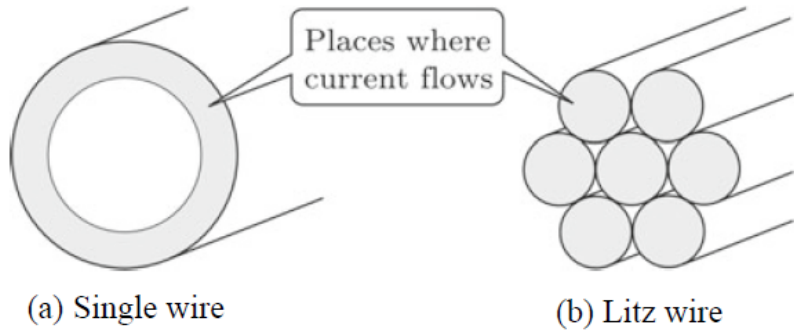


**Fig 2.8: Comparison of Current through a Solid Conductor and Litz Wire<sup>[4]</sup>**

For Litz wire, the DC resistance can be calculated as<sup>[2]</sup>

$$R_{WDC} = \frac{4 \rho_w l_w}{k\pi d_{str}^2} = \frac{4 \rho_w l_T N_l}{k\pi d_{str}^2} \quad (2.10)$$

Similarly, the AC resistance can be calculated as<sup>[2]</sup>:

$$R_{WDC} = \frac{4 \rho_w l_w}{k\pi} \left( \frac{l}{d^2} + \frac{\pi^3 (5N_{ll}^2 - 1) d^4}{2880 \delta^4 p^2 k^2} \right) \quad (2.11)$$

Further clarification has also been provided in the methodology section.

## 2.5 Coil Design

For defining the magnetic field of the WPT and its efficiency, the shape and materials of this pair of components are critical. The compensation networks' configuration will also be determined by the electrical properties of the coils. The coils' shape and arrangement must be determined through a lengthy design procedure that takes into account both economic and electrical considerations. To begin with, the usage of particular materials to work at high frequencies increases the cost of these coils; as a result, the length of the cables used for the turns and the size of the ferromagnetic parts should be carefully evaluated. Self-inductance, quality factor, and mutual inductance are affected by the geometry of the coil.

Higher quality factors of the coils can improve efficiency by up to 20%. For circular coils, even the dimension of the coil and the distance between the coils affect efficiency. The addition of ferrite cores aids in the increase of efficiency. The consequences of misalignments and displacements on coils need to be thoroughly studied and designs can also be made robust against such deviations.<sup>[2]</sup>

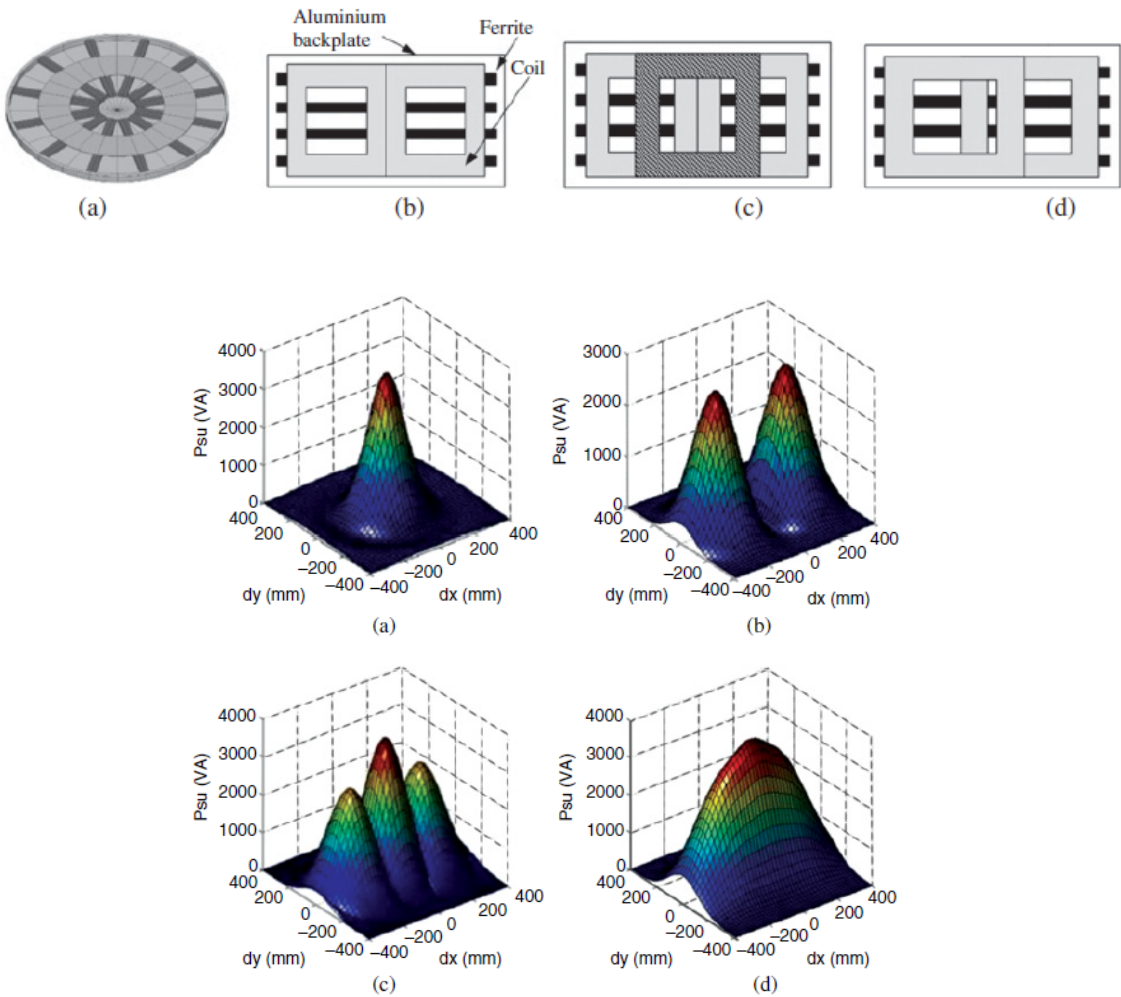


**Fig 2.9: Four Different Coil Topologies and the Respective Output Power Variation with the Position<sup>[5]</sup>**

## 2.6 Compensation Networks

In contrast to pure inductive charging, magnetic resonance chargers utilize compensation networks to maximize the power transfer between the primary and secondary. The compensation networks are the circuits that enable the transfer of power at resonance conditions. The parasitic capacitance between the coils is not enough to ensure resonance at the operational frequency range. Such compensation networks are used both on the primary and the secondary sides so that resonance occurs on the sending and receiving sides.

The system can act as a CV or CC output in some compensating topologies. This means that the wireless charger can withstand significant variations in electrical load, which are frequent during the charging process. Therefore, complex control systems can be avoided in the wireless charging of vehicles. As a result of this configuration, the losses associated with the power converters are reduced, and the overall system efficiency (including that of the power converters) is enhanced.

The simplest form of the compensation network is a single capacitor that may be connected in parallel or series.

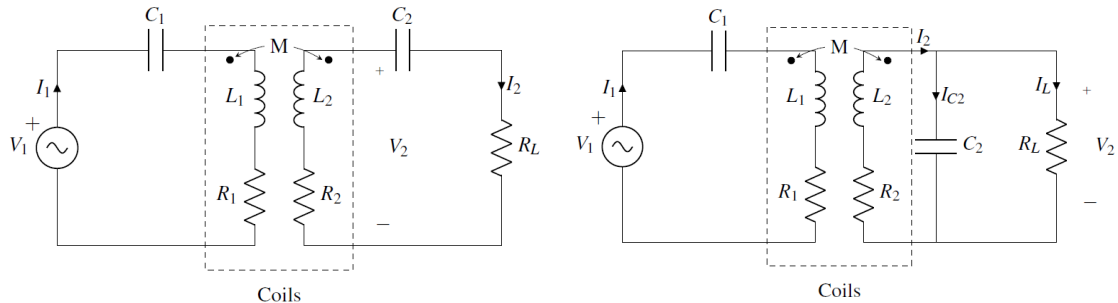


Fig. a

Fig. b

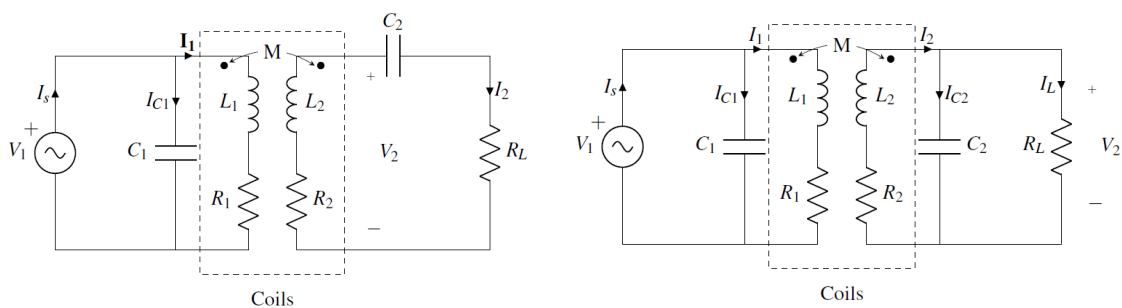
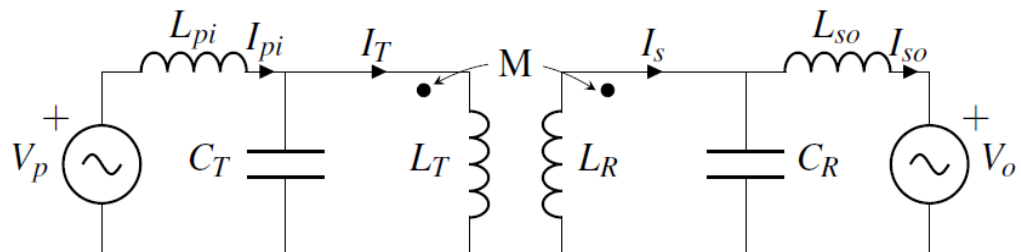


Fig. c

Fig. d

**Fig 2.10: a) Series-Series (S-S) Compensation, b)Series-Parallel (S-P) Compensation, c) Parallel-Series (P-C) Compensation, d) Parallel-Parallel (P-P) Compensation<sup>[2]</sup>**

All of the compensation networks shown above are known as mono resonant circuits consisting of a single reactive component i.e. capacitor. But multi-resonant circuits that use more than one reactive component are capable of increasing stability against the disturbances and improving coil efficiency even when coil misalignment occurs.



**Fig 2.11: LCL Compensation Network Topology**

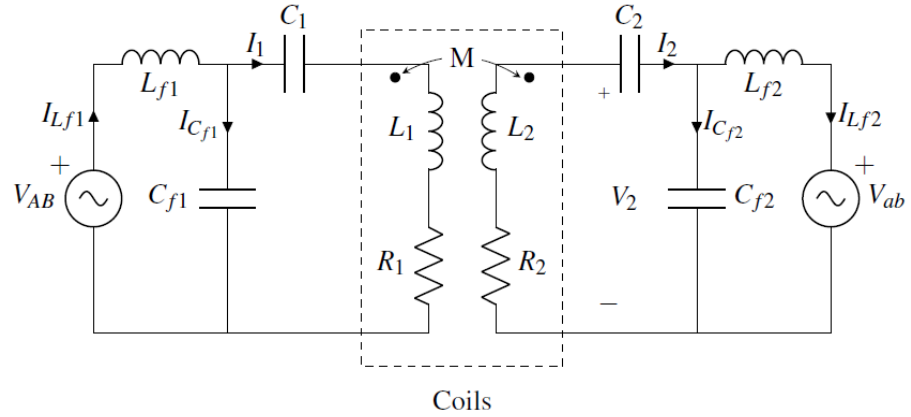


**Fig 2.12: LCC Compensation Network Topology**

## 2.7 Half-Bridge Inverter

An inverter is a device that takes a DC source as the input and outputs AC voltage. A half-bridge inverter consists of two switches that are alternately turned on and off. The diagram of a half-bridge inverter is shown in the figure below:

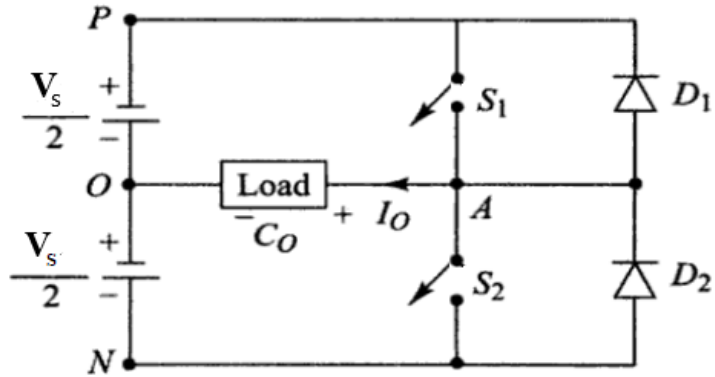


**Fig 2.13: Half-Bridge Inverter** <sup>[6]</sup>

$S_1$  and  $S_2$  are the two switches that are connected to the source voltage. The load is connected between the switches and the midpoint of two voltage sources. Diodes  $D_1$  and  $D_2$  are included to allow gradual discharge of current in the case of inductive loads. When  $S_1$  is ON,  $S_2$  is turned OFF and the current flows in the direction as shown. The voltage across the load is  $0.5 V_s$ . When  $S_1$  is turned off and  $S_2$  is turned ON, the current through load reverses and so does the voltage. Thus, the voltage across the load is  $-0.5 V_s$ . In this way, a half-wave inverter is operated. The switches are replaced using power electronics components such as Metal Oxide Semiconductor Field Effect Transistor (MOSFET) or Insulated Gate Bipolar Transistor (IGBT).

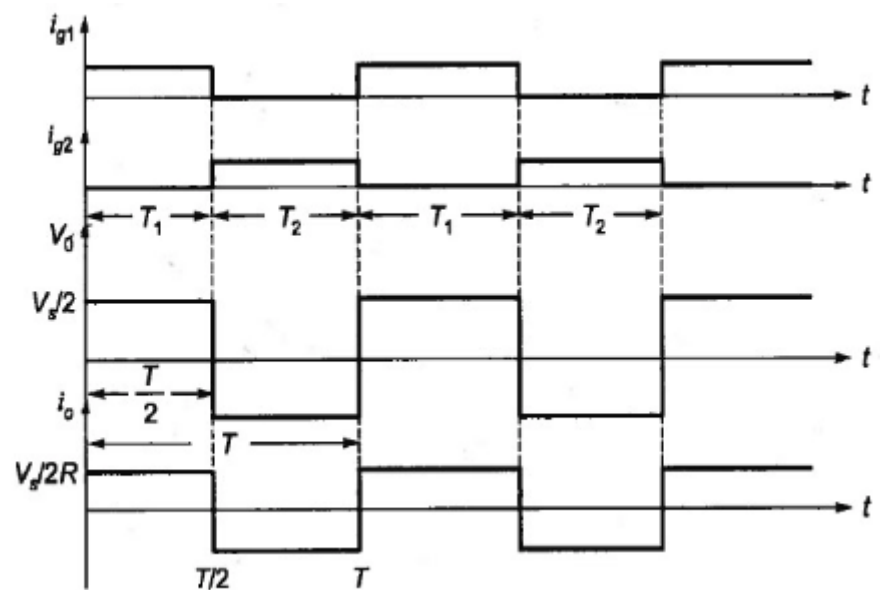


Fig 2.14: Waveforms of the Output Voltage of the Half-Bridge Inverter<sup>[7]</sup>

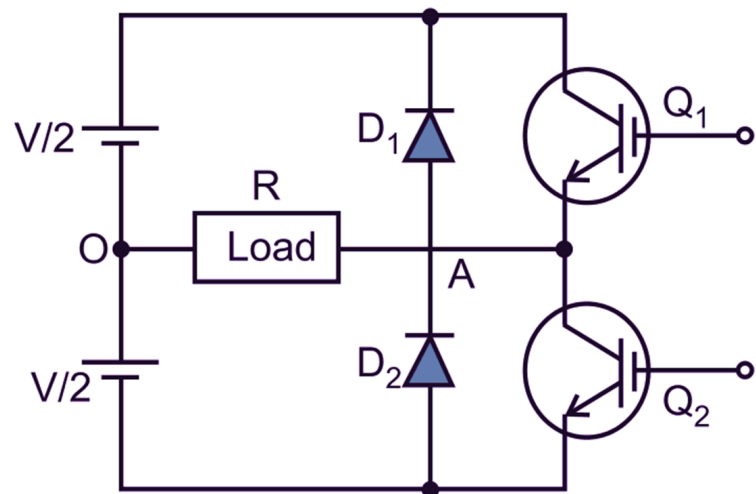


Fig 2.15: Half-Bridge Inverter Implemented with IGBT<sup>[8]</sup>

## CHAPTER THREE

### LITERATURE REVIEW

Recent market projections for wireless EV charging markets in transportation applications are encouraging. Consumer aversion to the inconvenient nature of plug-in wires, the requirement for charging infrastructure, and attributes like efficiency and dependability are projected to drive overall demand for wireless EV charging. People who are transitioning to electric vehicles from petroleum have continued to increase and this has opened up market prospects for wireless EV charging. North America and Europe are the leaders in terms of both EVs and wireless charging applications. EV Manufacturers and wireless-EV-charging providers have come together to better ensure niche viability and commercial reliability.<sup>[2]</sup>

Some of the major wireless EV charging solution providers are as follows:

- a. WiTricity: It was created in 2007 at MIT and used magnetic resonance techniques to provide wireless charging solutions. It works together with several EV manufacturers to develop wireless charging for them. It provides outputs ranging from 3.6-11kV with an efficiency of 90-93%.
- b. Qualcomm: “Halo” tech developed by Qualcomm from the University of Auckland forms the foundation for dynamic EV charging. They use magnetic resonance technology and are capable of bidirectional power transfer. They provided charging solutions ranging from 3.3 to 20kW at efficiencies greater than 90%. Recently, it was acquired by WiTricity.
- c. EVATRAN: It is a successful wireless charging system operating in the market. Their plugless units have supplied over 1 million trouble-free charge hours since the company's first production system was shipped in early 2014.
- d. Apart from that, car manufacturers like BMW, Audi, Mercedes-Benz, etc have confirmed the adoption of such technology to provide wireless charging solutions.

Apart from this, numerous research works have been carried out for wireless EV charging and the findings have been briefed in the following section. Timilsina et al. used a very limited and primitive approach to conduct wireless energy transfer focusing only on the power electronics circuit neglecting the coil design and compensation network configuration obtaining maximum efficiency of only about 10%<sup>[9]</sup>. El-Shahat A. et al. implemented a 3D model of inductive charging using square coils to obtain maximum efficiency of about 60% at very high frequencies.<sup>[10]</sup> Asa E. et al. et al. introduced a novel AC to AC WPT for charging EV without additional converter stages and closed-loop control that had an efficiency of 89%, THD 1.5%, and nearly unity pf. <sup>[11]</sup> A 100W wireless charging system for electric bicycle batteries was introduced along with a method for improving the overall power conversion efficiency was introduced by Pellitteri F. et al. Using circular planar coils and resonant frequency of about 100kHz, they were able to obtain an overall frequency of about 90.8%. <sup>[12]</sup> Kwan et al. demonstrated the design and construction of inductive power transfer (IPT) at 6.78 MHz with a dc-dc battery efficiency of 65.6% up to a gap of 17 cm.<sup>[13]</sup> Miller et al. presented a novel analysis process for wireless charging technology in which primary-side power regulation is selected and developed to minimize the complexity, size, and cost concurrently retaining the scalability

features.<sup>[14]</sup> Thrimawithana et al. exhibited a primary side control technique for IPT that requires a controller only on the sending side to effectively control the amount of power transferred.<sup>[15]</sup> Bosshard et al. have put light on the optimization of the IPT coil system with regard to efficiency and area-related power density depending upon the electric vehicle applications. Valid IPT designs are derived with  $\eta$ - $\alpha$ -Pareto optimization for the prototype of 5kW capacity.<sup>[16]</sup>

Therefore, these were the pieces of literature that were reviewed before we moved on to the design and implementation process.

## CHAPTER FOUR

### METHODOLOGY

Our project aims to implement Wireless Power Transfer(WPT) between two coils separated nearly 20 cm apart. The design process was completed in two major phases:

1. Software Simulation
2. Hardware Implementation

The simulation of the arrangement is done in simulation software like MATLAB, Multisim, and COMSOL Multiphysics. The simulation of the magnetic field was done in COMSOL, while the control system for the setup was done in MATLAB and Multisim for the study and tweaking of the system to be designed.

#### **4.1 Software Simulation**

The main aim of the software simulation is to select and design the appropriate topologies, and control mechanisms. In the simulation phase, various tasks were completed and finally, the whole process had to be reconsidered for the hardware implementation due to cost limitations and unavailability of the components required. The major tasks performed in this phase are chronologically listed as:

1. Selection and Design of Coil
2. Design of Circuits
3. Complete Circuit Simulation
4. Redesign Due to Hardware Limitations

##### **4.1.1 Selection and Design of Coil**

For the design of the coil, firstly the frequency of coil current has to be selected considering practicability and ferrite cores properties. Higher frequency is found to be favorable to lower the magnetic flux density around the coils and magnetizing currents. For this project, we have tried maximizing the frequency while staying within the technical limits. The limiting factors of the frequency are found as:

- Switching speed of Timers, MOSFETs, and Diodes
- Iron losses in the cores and the skin effect in the coils
- Harmonics of gate driving transformer
- Safety limits and standards

The frequency is selected as per SAE J294, IEC 61980, and ISO 19363 standards, which is 85kHz. This is the frequency of alternating current through the coil, the frequency of the magnetic flux, and the EMF at the terminals of the coils.

The steps carried out in the coil part design are:

1. Core Selection
2. Conductor Selection
3. Coil Design

#### 4.1.1.1 Core Selection

The coil design consists of the design of the transmitter and receiver coil along with the selection of the shielding materials. The shielding was introduced to block the magnetic field from diverting away from the receiver thus improving the coupling factor which also slightly increased the inductance of the coil. For shielding, the appropriate shielding material should be selected to minimize the core losses and stay within the flux saturation limit.

Various types of materials were examined in the simulation for the selection of the core. Going through the datasheet, the losses at the frequency to be operated was compared, and chosen one with acceptable characteristics. Considering the available materials, the family of MnZn cores is found to be suitable for this project. Mn60 core of these type is selected due to its properties as shown for our application:

**Typical Properties**

<b>Initial Permeability</b>	<b>6500</b>
<b>Maximum Permeability</b>	<b>8500</b>
<b>Saturation Flux Density</b>	<b>4500 Gauss</b>
<b>Remanent Flux Density</b>	<b>800 Gauss</b>
<b>Coercive Force</b>	<b>0.08 Oersted</b>
<b>Curie Temperature</b>	<b>170°C</b>
<b>dc Volume Resistivity</b>	<b>500 ohm-cm</b>
<b>Bulk Density</b>	<b>4.8 g/cc</b>

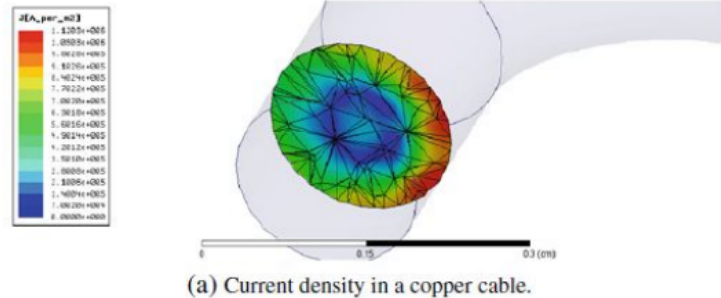
However, each type of MnZn core has different characteristics, which are easily available to procure, and are also acceptable.

#### 4.1.1.2 Conductor Selection

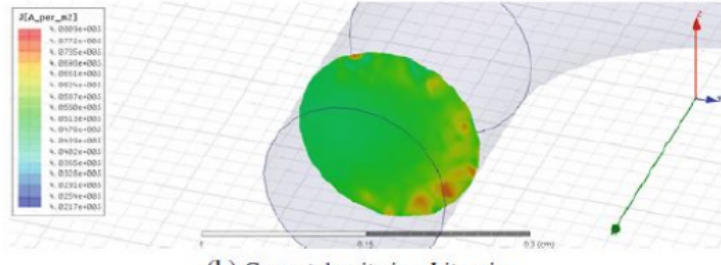
For winding, the copper conductor is chosen due to its superior conductivity and considering space constraints. However, the solid conductor of rated current couldn't be used due to the flow of high-frequency currents, offering higher AC resistance. Thus for high frequency, Litz wire (i.e stranding of small conductors, each insulated from the other) has to be used with appropriate sized conductors. The conductor selection can be done from various analyses and simulations giving some variation depending upon the method used. For our project, as the frequency of the current is 85kHz, general guidelines are followed to obtain the size of the Litz wire to be used.

Operation frequency range	AWG	Diameter (mm)
60 Hz to 1 kHz	28	0.3211
1 kHz to 10 kHz	30	0.2546
10 kHz to 20 kHz	33	0.1798
20 kHz to 50 kHz	36	0.1270
50 kHz to 100 kHz	38	0.1007

Thus, the Litz wire with each strand of size 38 AWG i.e 0.1007 mm diameter is chosen for our project.



(a) Current density in a copper cable.



(b) Current density in a Litz wire.

**Fig 4.1: Distribution of Current Density in (a) Copper Cable, and (b) Litz Wire<sup>[2]</sup>**

As we can see from the figure, the current density in the solid conductor is concentrated towards the surface of the conductor giving a less effective area. The uniformity of current density is improved in the Litz wire, reducing the AC resistance of the wire.

#### 4.1.1.3 Coil Design

After the selection of the core and conductor, the coil design is the next necessary step. The shape, number of turns, and topology are the parameters to be determined for the design of the coil. The coil design is done by first setting the requirement of the coil, and then calculating the parameters to fulfill the requirement. These requirements are listed as:

- Receiver Voltage: 84V RMS
- Flux Density around Coils: Less than 80mT (Considering safety)
- Size of coils: less than 40cm X 40cm (Size of scooter base)
- Magnetizing current: less than 5A
- No breakdown and arcing between and within coils

As there are no straightforward steps to approach the coil design process, it is done by hit and trial in Comsol Multiphysics software. Various coil shapes circular, pancake, and rectangular were tried and the number of turns was varied to get the required result. The designs with better coupling factor and higher inductance are preferred for better efficiency and less magnetizing current.

Finally, the annular coil design with 45 turns on the primary side and 16 turns on the secondary side is finalized for the project. The other parameters for the coil are obtained from the Comsol Multiphysics as:

### Primary Coil:

- Number of turns: 45
- Coil Inductance: 582.6582185 uH
- Coil Resistance: 75.7613759647 mOhm
- Mutual Inductance: 44.48511 uH
- Coupling factor: 0.07634855

### Secondary Coil:

- Number of turns: 16
- Coil Inductance: 159.96197 mH
- Coil Resistance: 13.561247 mOhm
- Mutual Inductance: 44.48511 uH

The selected coil design is represented in 3D space as:

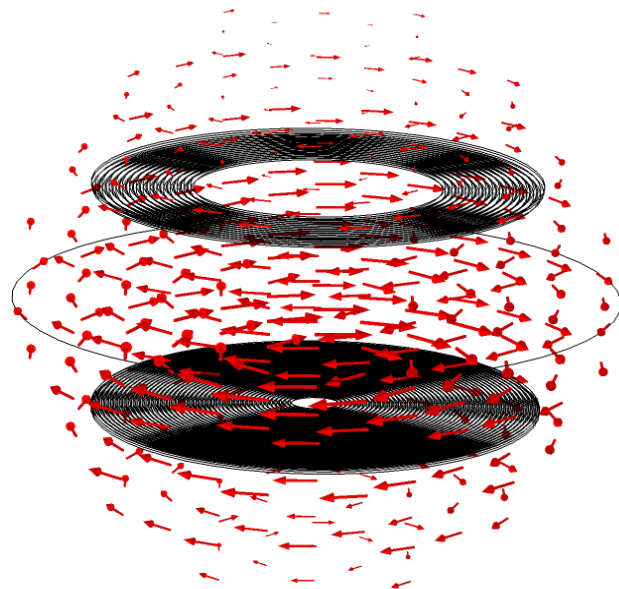


**Fig 4.2: Selected Coil Design**

The figure shows the transmitter coil at the bottom and the receiver coil at the top. The electric and magnetic fields are represented by red and blue arrows respectively. A circular cylindrical core is implemented on both primary and secondary sides with the same size as the coil.

#### **4.1.2 Design of Circuits**

The design of the circuits is another major step carried out in the software simulation phase. Firstly, we developed the complete block diagram of the system to obtain the required functionality and then the circuits for each block were developed in Matlab.

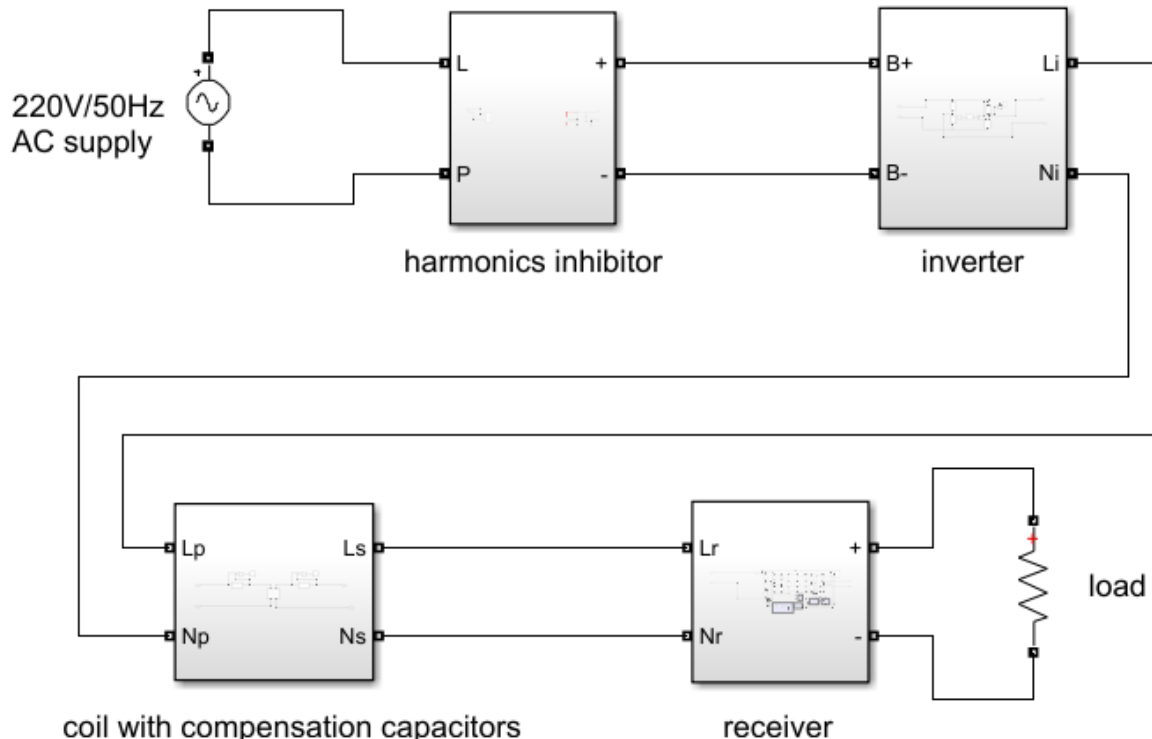


**Fig 4.3: Schematic Diagram of the System**

These blocks are chosen to perform a specific task and feed another block fulfilling its input requirement. The blocks used in the system are:

1. Harmonic Inhibitor Block
2. Inverter Block
3. Coil Block
4. Receiver Block

The circuit diagrams for each block were developed and tested separately, and finally integrated.

#### 4.1.2.1 Harmonic Inhibitor Block

The main function of the Harmonic Inhibitor Block is to convert the power from the utility grid at 220V, 50 Hz AC to DC at 400V while minimizing the input current harmonics to the acceptable limits. The DC value of 400V is chosen from the coil design to minimize the conductor cost and voltage rating of switching devices.

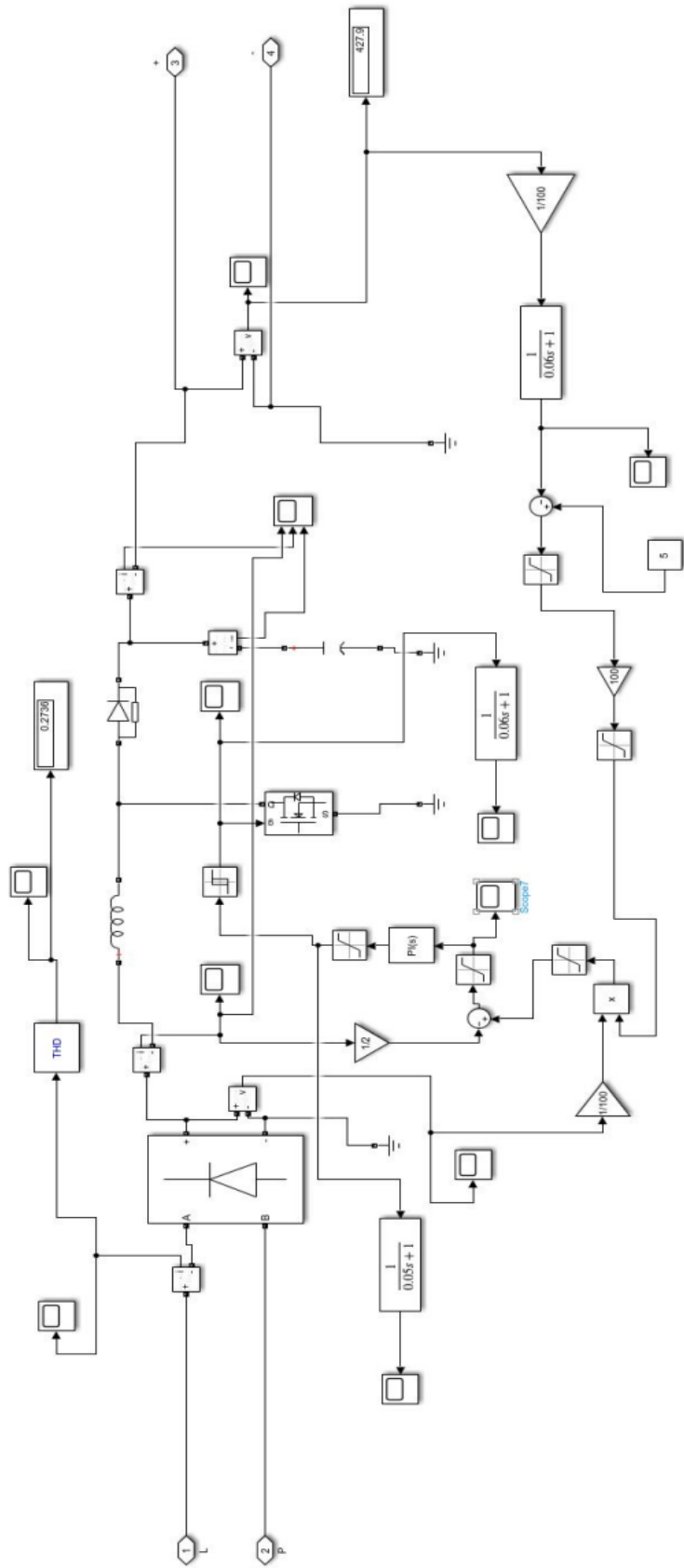


**Fig 4.4:** Harmonic Inhibitor Circuit

The harmonic inhibitor circuit uses the current controlling arrangement to minimize the input current harmonics. The current reference is taken from the voltage waveform, which is assumed to be harmonic-less i.e perfectly sinusoidal. The hysteresis current control mechanism is used for switching the MOSFET. Also, a feedback loop is implemented in the circuit to regulate the output voltage. As the inverter circuit may not act as a linear load, voltage fluctuation may occur, which can be reduced by introducing closed-loop feedback. The voltage regulation is done by controlling the magnitude of input current depending upon deviation from reference voltage using PI controllers. The parameters for PI controllers are tuned by hit and trial, thus obtaining the required functionality.

#### 4.1.2.2 Inverter Block

The constant DC output is then converted to alternating voltage using the inverter block. The use of a perfect sinusoidal inverter is ideal but is not implemented in our project due to the complexity and efficiency of such inverters. For the use of SPWM, the frequency of the gate signals required was found to be near 1MHz, which is found to be very costly using expensive MOSFETs and Oscillators. Hence, considering those points, the square wave inverter is selected for our project. However, for square wave inverters, the use of a full-bridge arrangement is better, for which the four gate signals, with a pair of them in the same phase, need to be generated. Using a half-bridge arrangement is also suitable for the project, which requires only two MOSFET and two gate signals. For simplicity and efficiency (less loss in less number of switches), the half-bridge arrangement is chosen for our project.

Thus, the schematic diagram of the inverter block is as follows:

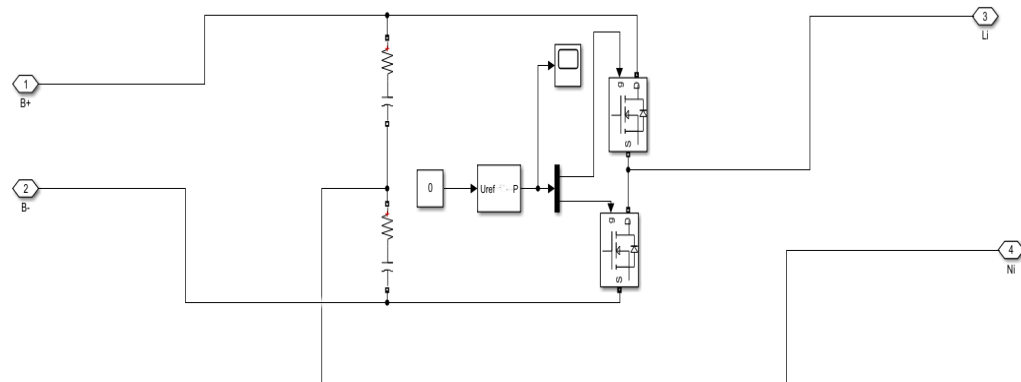


**Fig 4.5: Inverter Circuit Diagram**

#### 4.1.2.3 Coil Block

The coil block consists of the transmitter and receiver coils along with the compensation networks. Among various compensation topologies(i.e series-series, parallel-series, parallel-parallel, series-parallel topologies), the one is chosen depending

upon the application and the response required.

We tested the various topologies under no-load, full-load, and partial-load conditions, and one staying within the safe value of current and voltage limits was selected. For our system, we have found parallel-series compensation suitable considering no-load current minimization. However, due to the use of square waves, the current spike through the inverter was seen as the capacitor is connected in parallel on the transmitter side. To eliminate this problem, the series inductor is inserted as a filter to limit the current to a safe value. Thus, the schematic diagram of the coil block is constructed as follows:

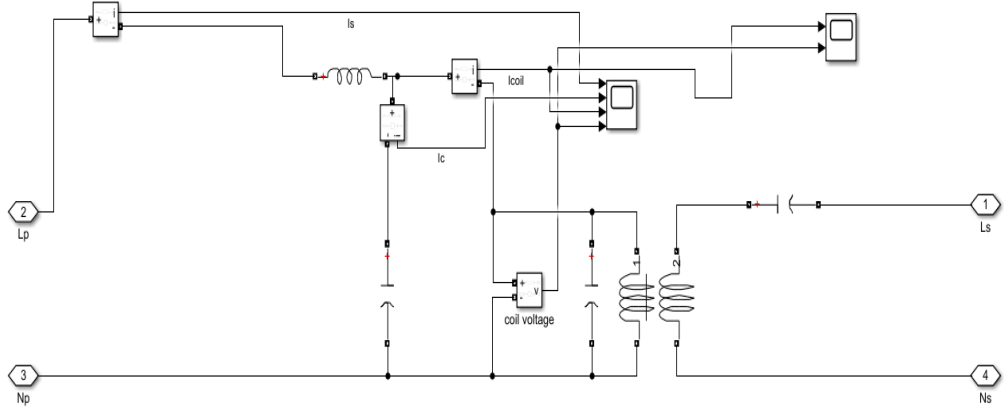


**Fig 4.6: Schematic Diagram of Coil Block**

#### 4.1.2.4 Receiver Block

The power from the receiver coil is then converted to the voltage of the required level by using the Receiver Block. As the voltage received at the receiving side is sinusoidal, it needs to be converted to DC using the rectifier and the voltage regulating circuit. The AC to DC conversion is generally done by simply implementing the full-bridge rectifier, but the harmonics in the current may arise due to the use of simple filters like capacitors. However, this problem does not arise in our case due to the use of compensators on the secondary side as the input voltage to the rectifier is not sinusoidal in a steady state.

The voltage regulation needs to be done because the coupling factor can change drastically between the coils every time due to imperfection in alignment/placement. The voltage regulation is done by using a simple Buck Converter in the feedback loop to obtain the constant DC output of the required value.

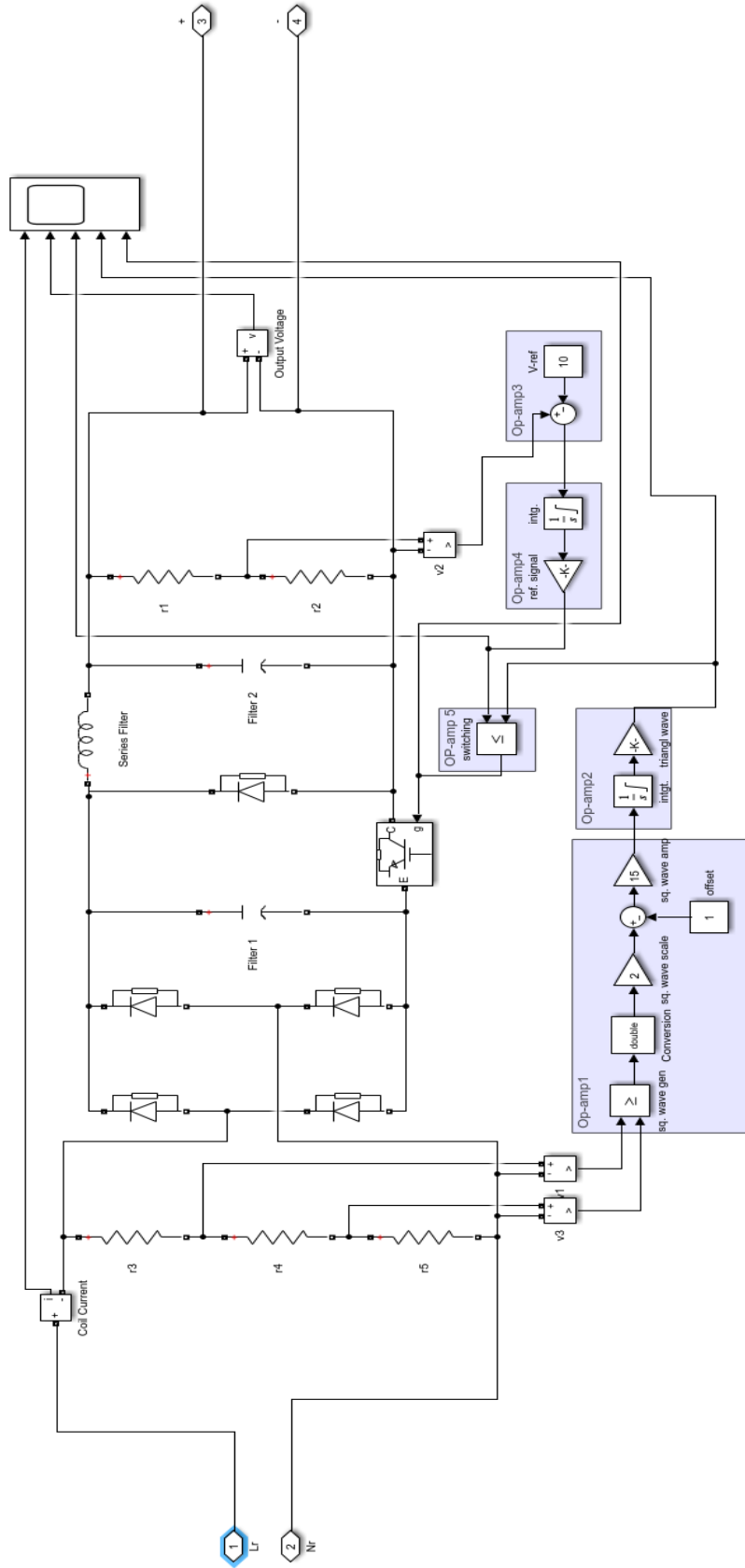
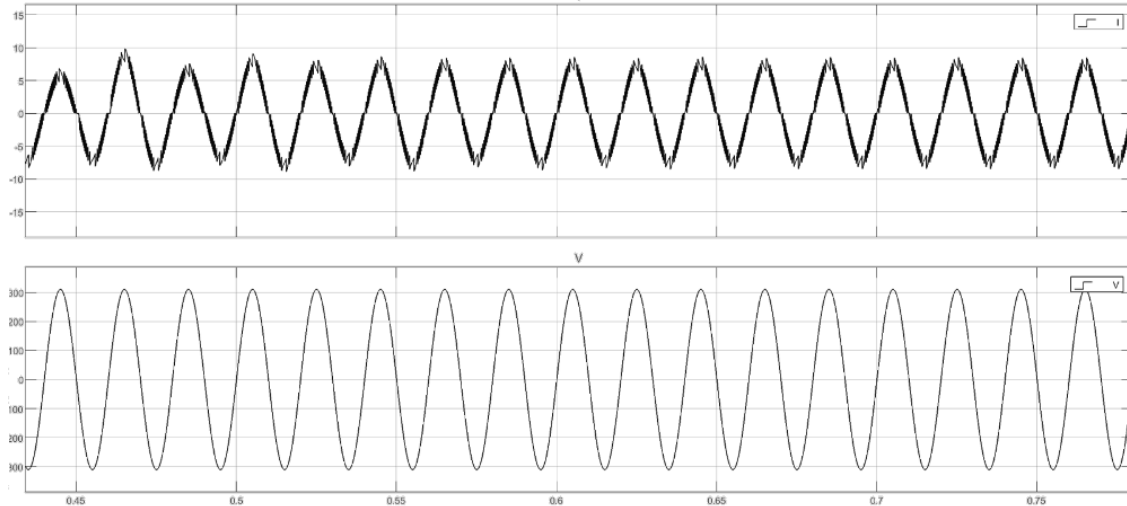


Fig 4.7: Schematic Diagram of the Receiver Circuit

As we can see in the schematic diagrams, the circuits are developed in Matlab while keeping the hardware implementation in mind. The use of Op-Amps was planned to be used for arithmetic operations while separate programmable ICs(like Microcontrollers) should be implemented for complex controlling mechanisms.

#### 4.1.3 Simulation Results

The circuit was integrated and simulated in Matlab until it reached a steady state. The input current and voltage waveforms are obtained as below:



**Fig 4.8: Input Current and Voltage Waveforms**

The upper waveform is of input current and the lower one is the input voltage waveform. As we can see, the input current is nearly sinusoidal, i.e reduced harmonics, and is in phase with input voltage.

Also, the output of the system is obtained as:



**Fig 4.9: Output Current and Voltage**

As we can see, the output of the system is maintained to the required value, i.e 84V

after a very short time. As we have used a resistor as our load, the nature of the current waveform is the same as the voltage waveform.

#### 4.1.4 Redesign Due to Hardware Limitations

The whole arrangement was completely designed and ready for hardware implementation. However, during the procurement of the hardware, it was found that the required components are not available in the local markets. The selected core and the coil were calculated to be too costly. Also, they need to be imported from foreign countries which was found to take too much time.

Hence, the objective of the project was then reconsidered so that it can be completed while staying within the economic limits and deadline schedule. The schematic diagram of the system was reconstructed, which is as shown below:

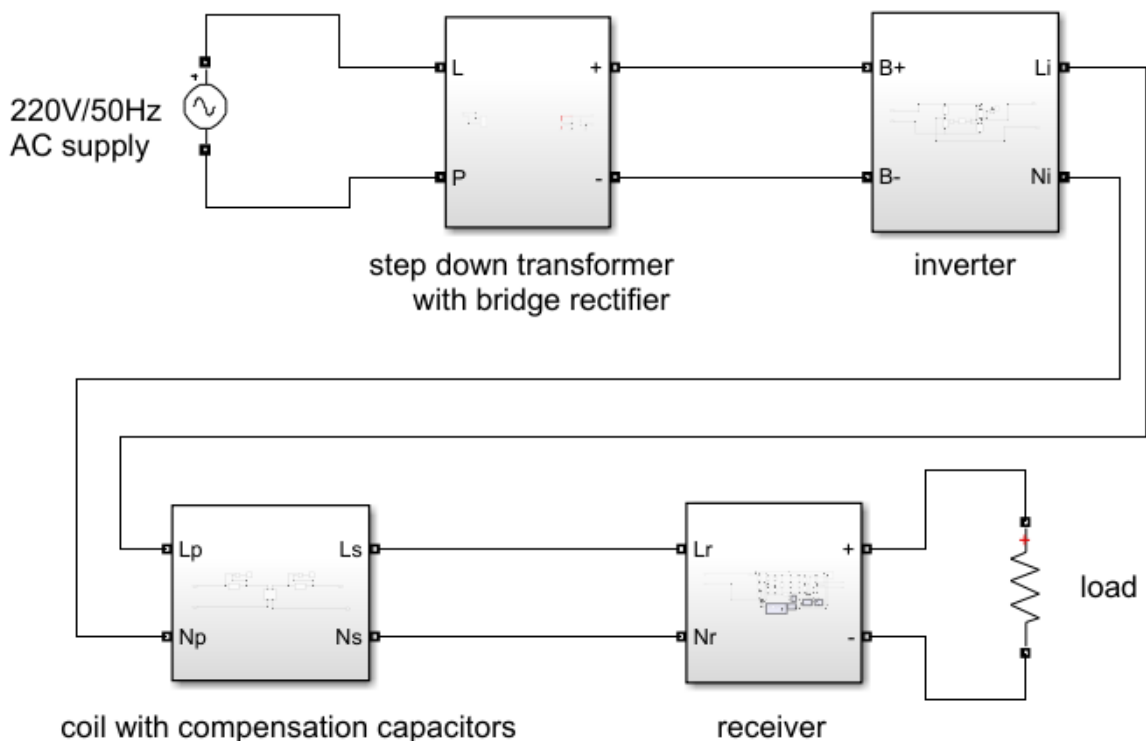


**Fig 4.10: Schematic Diagram of the Redesigned System**

Due to the unavailability of the core, the shielding was eliminated in the new system design. Due to this, the coupling factor and self-inductance are reduced. Thus the power rating of the system was also then reduced to 100W to reduce copper losses.

The major changes made in the new design are listed as:

1. Elimination of Harmonic Inhibitor Circuit
2. Elimination of Shielding Core
3. Change of Coil Design
4. Change in Compensation Topology
5. Change in DC output of AC to DC Converter
6. Elimination of Voltage Regulation in the Receiver Circuit

The changes made in the system are done considering the safety limits and the economic feasibility. However, some changes are the effect of the change on other parts of the system.

#### 4.1.4.1 Elimination of harmonic inhibitor circuit

As the harmonic inhibitor circuit is very complex and requires expensive components, they are replaced by a simple step-down transformer with a full bridge rectifier and a capacitor.

#### 4.1.4.2 Elimination of shielding core

Considering the cost of the core, the core is eliminated in the new design. This removes the feature of field shielding and reduces coil inductances. The change in magnetic field contour can be used to see the effectiveness of the shielding effect around the coils.

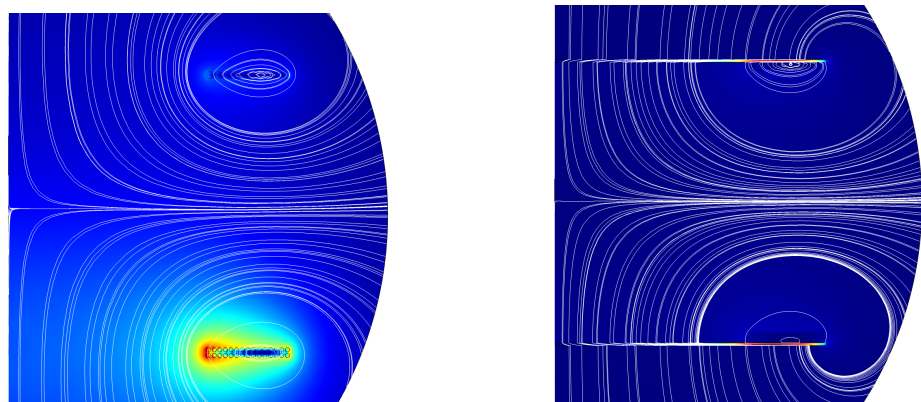


**Fig 4.11: Magnetic Field Contour Plot without Core (Left), and with Core (Right)**

#### 4.1.4.3 Change of Coil Design

After the elimination of the core, and the expensive copper cost of the previous design, the coil design was done again to minimize the copper cost and satisfy technical feasibility. Different valid coil designs were considered and the cost for each design was calculated (Fig 4.12).

For Im = 5A and K=0.079 => L1min = 682.6uH and L2min = 82.11uH							
Coil Design	N1/layer	Layer1	N2/layer	Layer2	Bmax[mT] @ 5A	M[uH]	R1[mΩ]
T30-10L2-2	15	2	5	2	50	36.29357925	78.0594148
T30-10L2-1	15	2	10	1	50	34.48053908	78.05940267
T50-10L1-2	50	1	5	2	50	30.65138826	79.0388174
T50-10L1-1	50	1	10	1	50	30.65138826	79.0388174

For V1=144V, V2=48V, P=1000, J=3A/mm <sup>2</sup>			
wire_d1[mm]	wire_d2[mm]	insulation[mm]	outer diameter[cm]
3	5	1	40

For copper density = 8.960 gm/cc					
Coil Design	Volume1[cc]	Weight1[kg]	Volume2[cc]	Weight2[kg]	Total Weight[kg]
T30-10L2-2	402.6798596	3.608011542	328.6578266	2.944774126	6.552785668
T30-10L2-1	402.6798596	3.608011542	302.0098947	2.706008656	6.314020198
T50-10L1-2	394.784176	3.537266217	328.6578266	2.944774126	6.482040343
T50-10L1-1	394.784176	3.537266217	302.0098947	2.706008656	6.243274874

**Results** | T30-10L2-1 is selected as it matches requirement, Symmetric, Less weight

**Fig 4.12: Cost Comparison Of Different Coil Designs**

Thus, the design of T30-10L2-1 (i.e 30 turns on the primary side with two layers stacking each of 15 turns and 10 turns on the secondary side without stacking) is selected.

#### 4.1.4.4 Change in compensation topology

As the coil parameters were updated, the efficient topology had to be found again. From the simulation of Matlab, considering the small changes in coupling factor, this time the series-series topology was found to be effective. Also due to the smooth current through the inverter (and perfect sinusoidal at the resonance), the current filter is then eliminated. The updated coil schematic diagram is as follows:

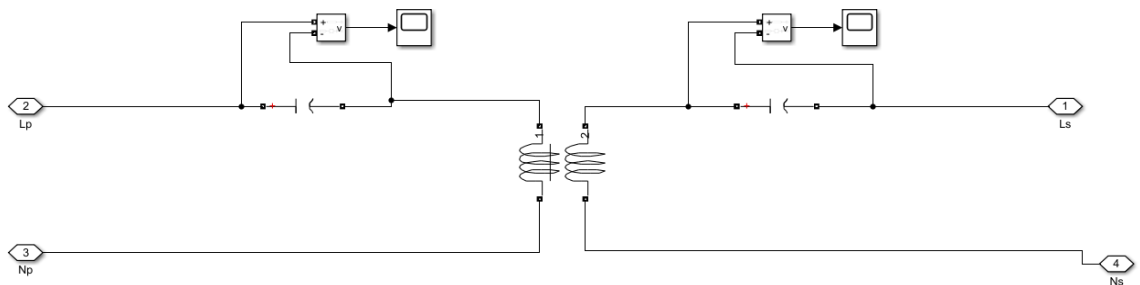


**Fig 4.13: Schematic Diagram of Coil Block for New Design**

The values of compensating capacitors were recalculated from the simulation using the updated coil parameters.

#### 4.1.4.1 Change in DC Output of AC to DC converter

Due to the reduction of the inductance of cores, the magnetizing current can increase dramatically if used with the same voltage as before. Thus to limit the copper cost, the magnetizing current had to be minimized. In the coil redesigning process, the lowered value of the square wave was found to be favorable and economic. The voltage of the square wave is reduced to 80V hence the output of the AC to DC converter (which is a simple transformer and rectifier in our new design) was reduced to 160V DC.

#### 4.1.4.1 Elimination of Voltage Regulation in the Receiver Circuit

Another change made in the system redesign is the elimination of voltage regulation in the receiver circuit. As the regulation circuit requires some circuits to control the gate signal at high speed, they are found to be expensive and thus were omitted. A simple resistor is implemented as a linear load on the secondary side without the application of any rectifiers and Buck converter thus feeding the perfect sine wave at the load.

Hence, after the complete design of the system in the software, the project is then implemented in hardware.

## 4.2 Hardware Implementation

Due to the unavailability of some resources in Nepal, we had to compromise on the design. Unavailability of MnO core (for 100kHz) and also the unfavorable situation for import of core we had to make a coreless transmitter and receiver. The main impact of coreless is a decrease in inductance so as mutual inductance. This eventually decreases magnetizing reactance and increases magnetizing current. To keep the same magnetizing current as for a cored transmitter we had to reduce the input voltage from 400V to around 90V. To keep the same current at the rated load in the coil we had to decrease power as voltage decreased, from 1kW to around 100W. Also, shielding was compromised.

We used a matrix board to fabricate our circuit for prototype purposes.

### 4.2.1 Transmitter Coil

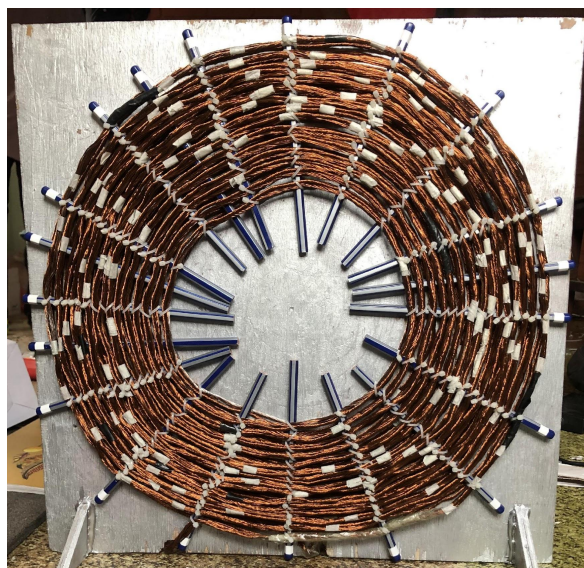


**Fig 4.14: Transmitter Coil**

The transmitter coil contains 2 layers. Each layer contains 15 turns of group wire. The group wire contains several thin wires. These thin wires are enamel-insulated copper wires. The outer diameter of the coil is 40 cm. The coil is supported by the silver-painted square wooden plank of 40 cm sides. These pencils are used in between the layers to provide insulation between layers. The group wire is supported by a wooden plank using zip ties. Inductance is found to be around 350 uH.

#### 4.2.2 Receiver Coil



**Fig 4.15: Receiver Coil**

The receiver coil contains a single layer. The layer contains 10 turns of group wire. The group wire contains several thin wires. These thin wires are enamel-insulated copper wires. The outer diameter of the coil is 40 cm. The coil is supported by the silver-painted square wooden plank of 40 cm sides. These pencils are used in between the layers to provide insulation between layers. The group wire is supported by a wooden plank using zip ties. Inductance is found to be around 40 uH.

#### 4.2.3 Transmitter Compensation Capacitor



**Fig 4.16: Transmitter Compensation Capacitor**

The transmitter compensation capacitor consists of 2 parallel aluminum foil plates rolled in a spiral shape. Dielectric in between plates is a layer of newspaper and polythene which has higher dielectric strength than air. Glue is used to stick newspaper, polythene, and aluminum plates together. The stranded thick copper wire connected with aluminum plates is taken out as a terminal. A watercolor tap is used to wrap the structure from the outside to minimize the deformation of the structure and the formation of air gaps inside the capacitor. Capacitance is made around 10nF and dielectric breakdown of 9kV.

#### 4.2.4 Receiver Compensation Capacitor



**Fig 4.17: Receiver Compensation Capacitor**

The receiver compensation capacitor is made from two capacitors connected in parallel. Each capacitor consists of 2 parallel aluminum foil plates rolled in a spiral shape. Dielectric in between plates is a layer of polythene that has higher dielectric strength than air. Glue is used to stick polythene, and aluminum plates together. The stranded thick copper wire connected with aluminum plates is taken out as a terminal. A watercolor tap is used to wrap the structure from the outside to minimize the deformation of the structure and the formation of air gaps inside the capacitor. Each capacitor is made at around 40nF with a dielectric breakdown of 6kV. Those two capacitors yield around 80nF while they are connected in parallel.

#### 4.2.5 Power Supply (Inverter)

The power supply is taken from the transformer. The transformer takes 50 Hz - 220 Vrms AC supply as input and produces 50 Hz - 117 Vrms AC supply as output. These outputs are fed to the rectifier. The transformer is used as an autotransformer to minimize the loading effect.

#### 4.2.6 Rectifier with Filter

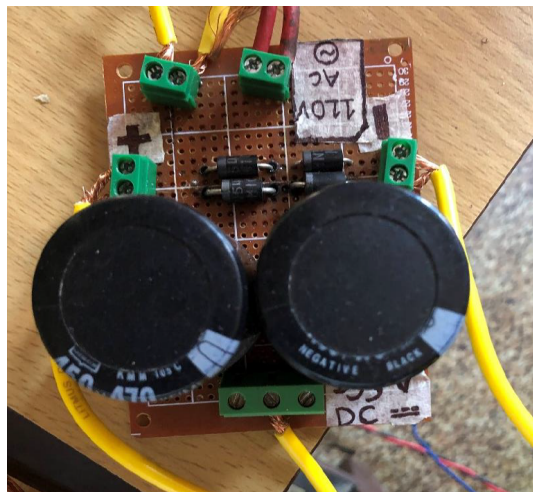


**Fig 4.18: Rectifier with Capacitor Hardware**

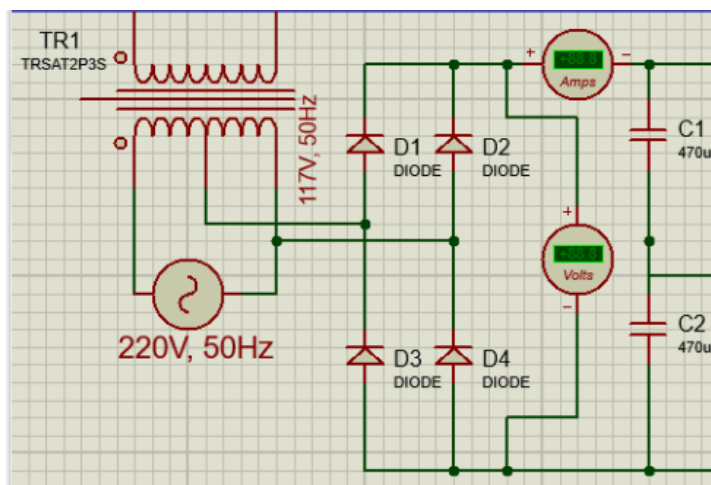


**Fig 4.19: Rectifier with Capacitor Schematic**

The rectifier is a bridge rectifier consisting of four 1N5408 diodes with a current rating of 3A. The output from the rectifier is pulsating DC around a peak of 166V. Two capacitors of rating 470uF/450V are connected in series. Pulsating DC is taken by these capacitors as in the figure and produces a low ripple DC output of around an average voltage of 165 V. The junction or node of two capacitor interconnections acts as the 0-reference or ground reference for inverter circuits. The positive terminal (denoted by '+' in hardware) produces around 80 V with ground reference. The negative terminal (denoted by '-' in hardware) produces around -80 V with ground reference. Ground reference is denoted by 'DC==' in hardware. The circuit is soldered on a matrix board. All the inputs and outputs are taken out by using Bornier on a matrix board.

#### 4.2.7 Inverter (Half-bridge)

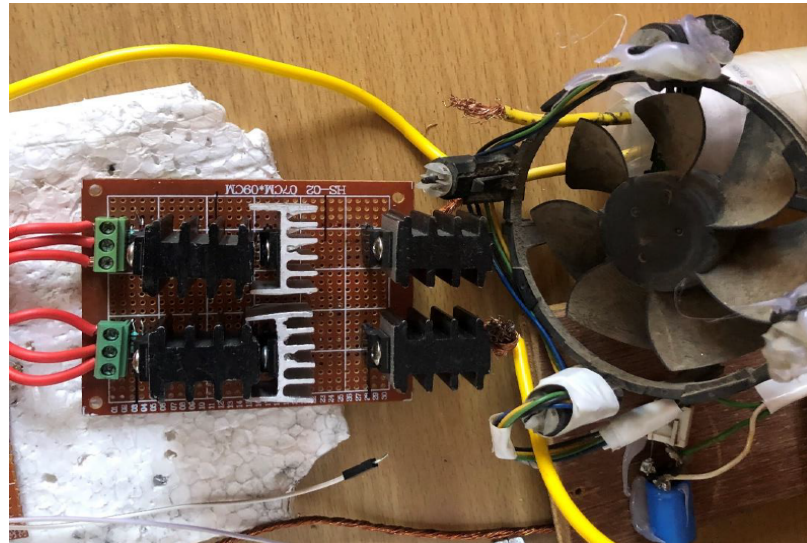


**Fig 4.20: Inverter Hardware**

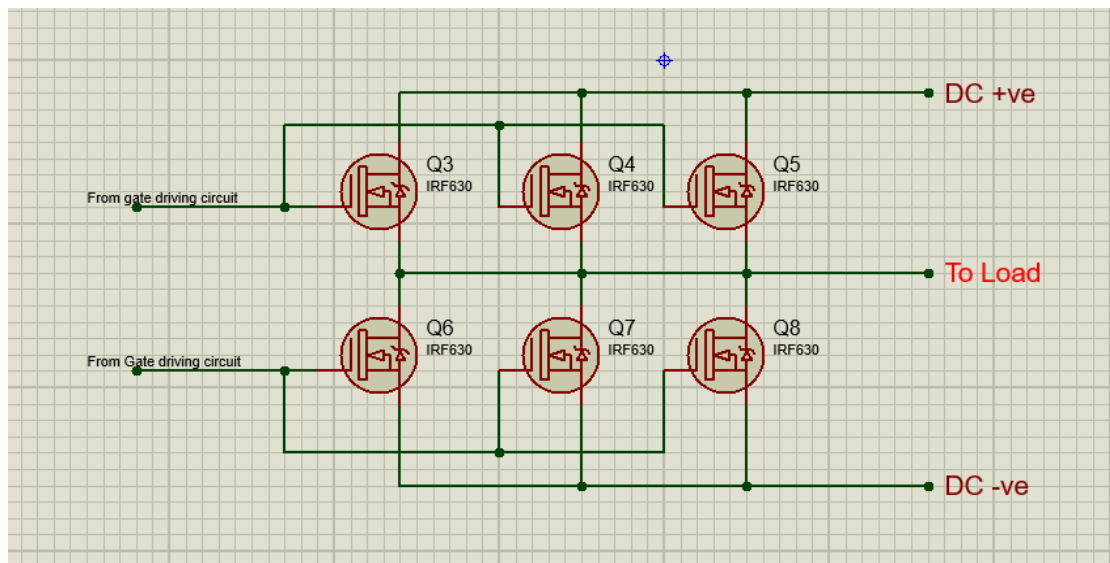


**Fig 4.21: Inverter Schematic**

The inverter consists of two groups of MOSFETS. Each group contains three IRF630 MOSFETS connected in parallel to increase the current rating and reduce loss. The current rating of IRF630 is 9A. So all together each group's current rating will be  $3 \times 9A = 27A$ . So the inverter rating is 27A. The voltage rating of IRF630 is 200V. The group's voltage rating becomes 200V. The inverter's voltage rating also becomes 200V. Each group contains a gate, drain, and source. The source of one group is connected with the drain of another group of MOSFETS. The positive from the rectifier circuit is connected with the drain of the uppermost group and the negative from the rectifier is connected with the drain of the lower group of MOSFETS. There are two gates to the inverter. One gate is the upper group of transistors and another is the lower group of

transistors. These gates require complementary square wave signals of around 10V to drive inverters. These square waves signal is given from the gate drive transformer. In hardware, the female pin header is soldered such that the MOSFET can be replaceable if damaged. The heat sink is used for every MOSFET to maintain temperature or cooling. A CPU fan is also used for cooling if excessive heat is produced in overload. Three-pin barriers are used for each group of transistors for the gate, drain, and source terminal.

#### 4.2.8 Gate Driver

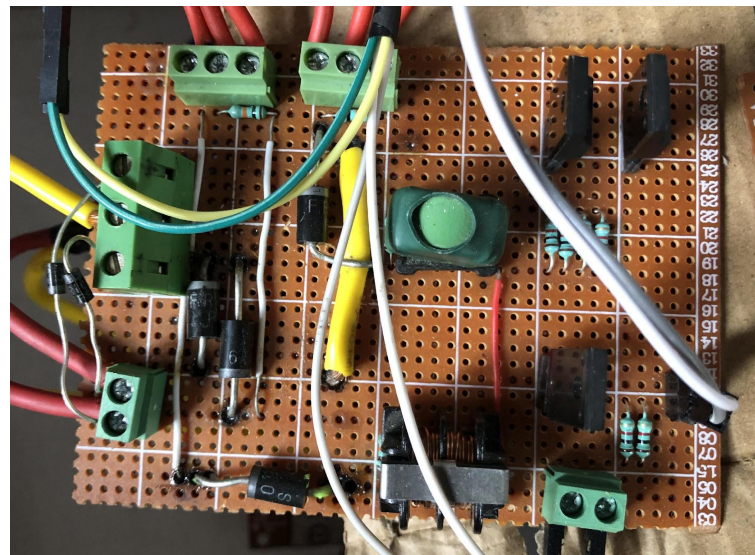


Fig 4.22: Gate Driver Hardware

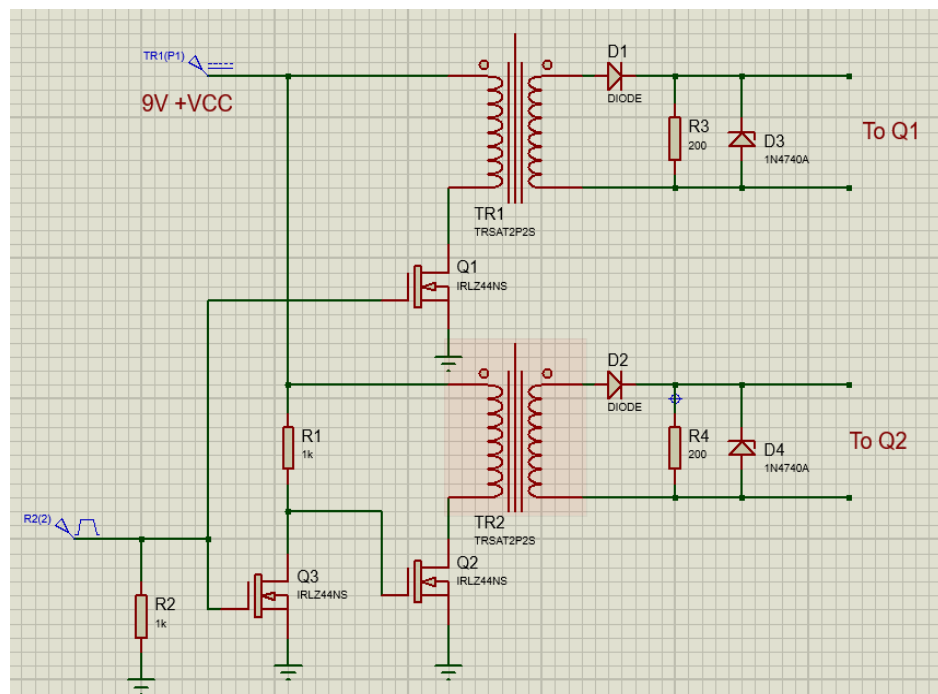
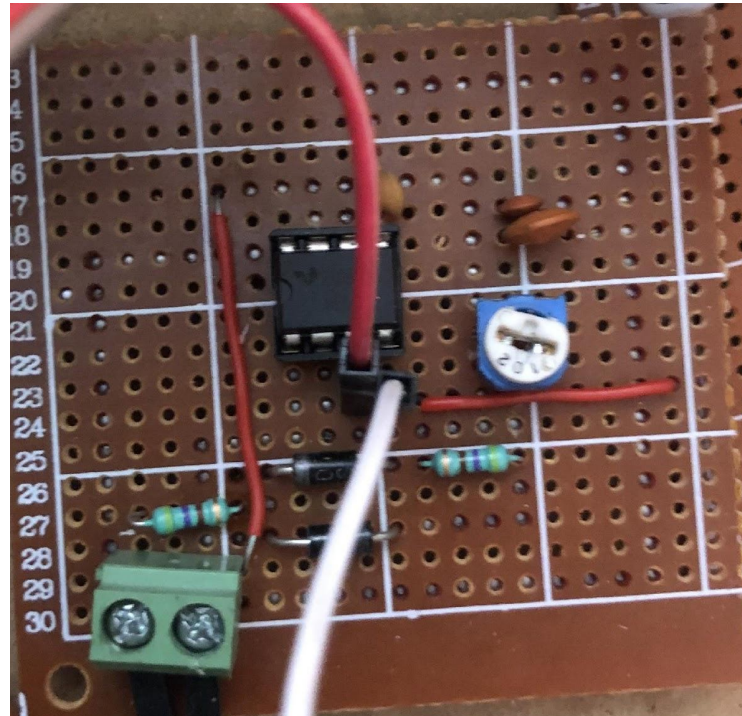


Fig 4.23: Gate Driver Schematic

Gate drivers consist of two gate drive transformers (more precisely toroidal transformers). The output of each transformer is connected with a shunt resistor of 200 Ohm to reduce equivalent output impedance and a zener diode of 12V reverse breakdown to protect MOSFET from pulses higher than 12V. Each gate drive transformer is connected between the 9V DC source and the drain of MOSFET. MOSFET operates a switching device. The Gate signal for upper MOSFET is directly given from the output of the oscillator. Gate signal for lower MOSFET if taken from the drain of an inverting

MOSFET which inverts the signals from the oscillator. All the circuits are soldered on a matrix board. All the inputs and outputs are taken from the borniers on matrix boards.

#### 4.2.9 Oscillator



**Fig 4.24: Oscillator Hardware**

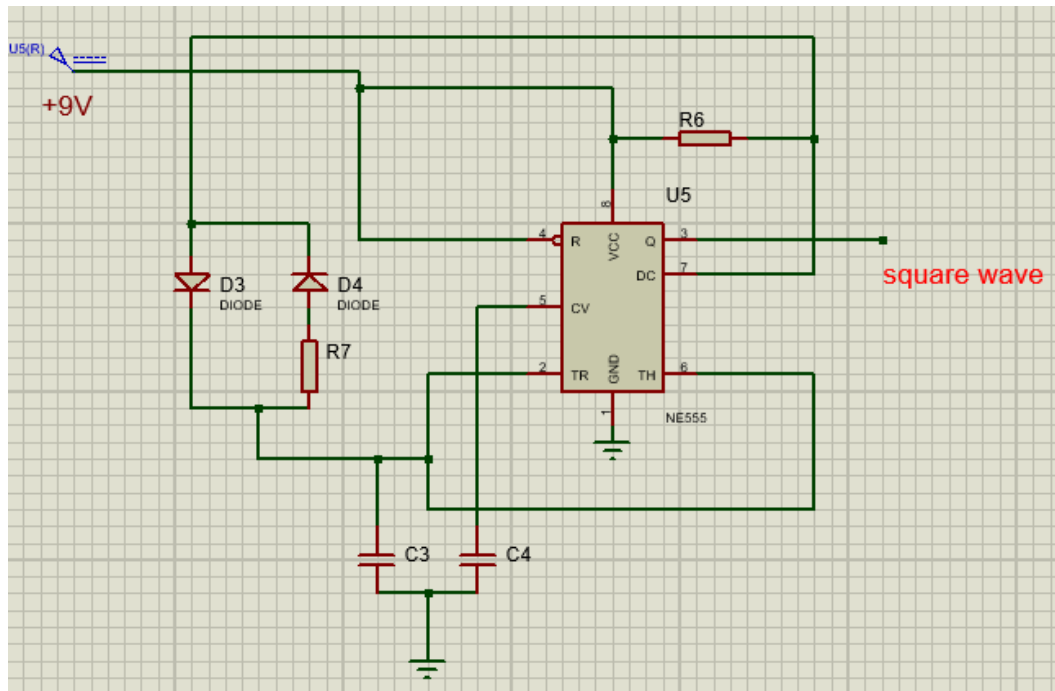


**Fig 4.25: Oscillator Schematic**

The oscillator is designed using a NE555 timer in astable mode. As in figure two Schottky diodes are used to make an output rectangular wave of duty cycle 50%. It

generates square waves up to 110kHz with amplitudes of around 8 V. Output from this oscillator is given to the gate driver. The circuit is fabricated on a matrix board. A 9V dc supply is given to the oscillator.

#### 4.2.10 Voltage Controlled Oscillator

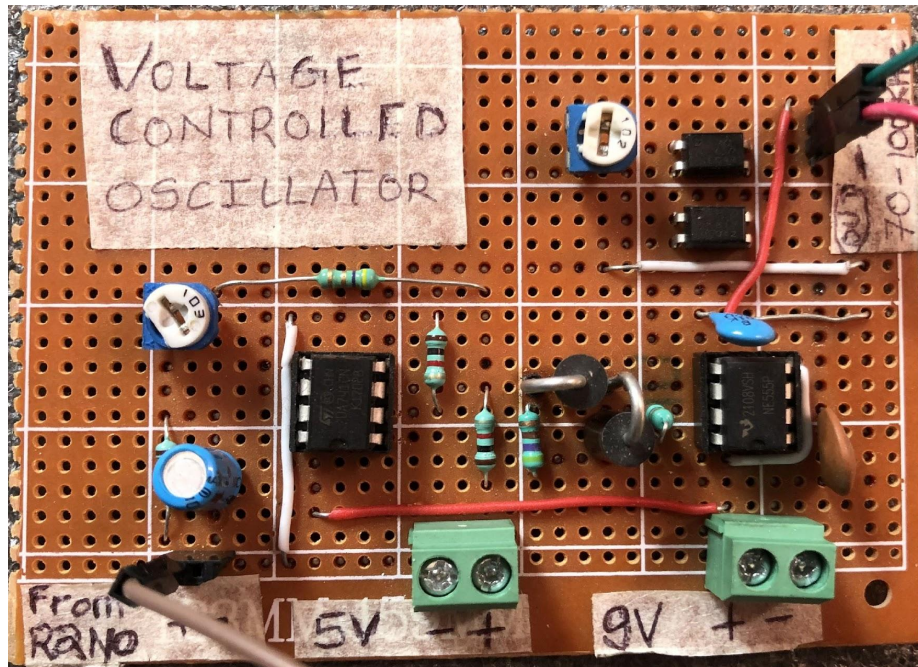


Fig 4.26: Voltage Controlled Oscillator Hardware

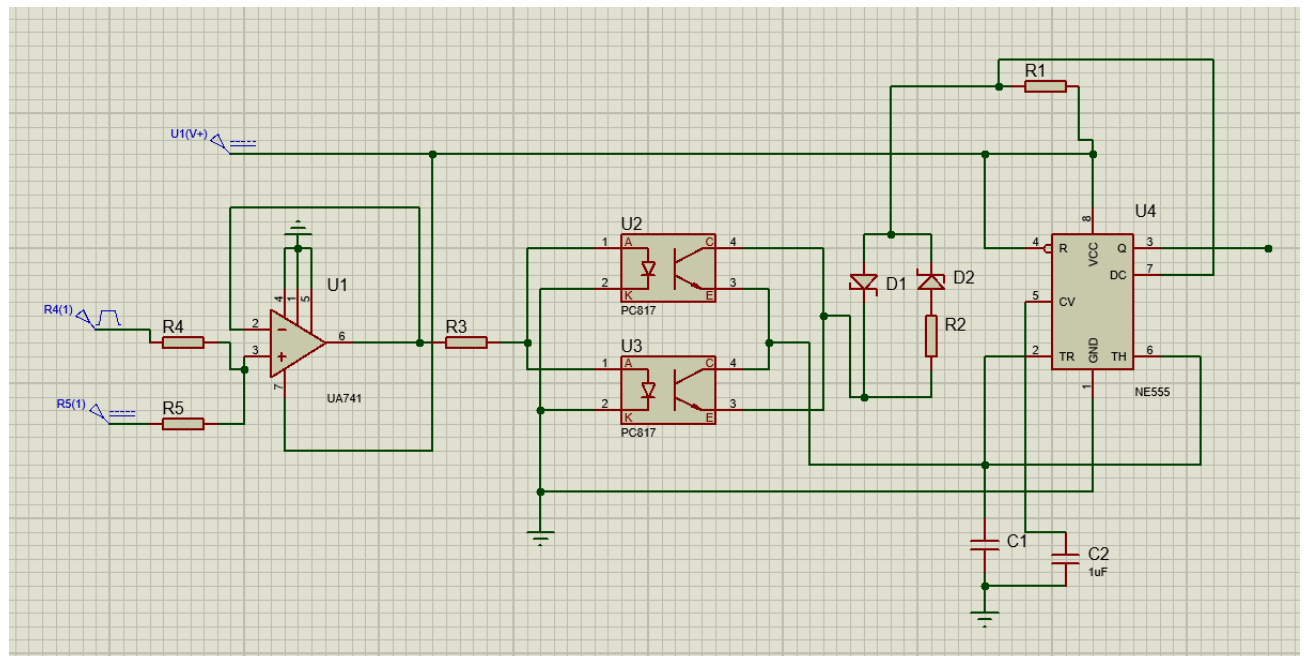
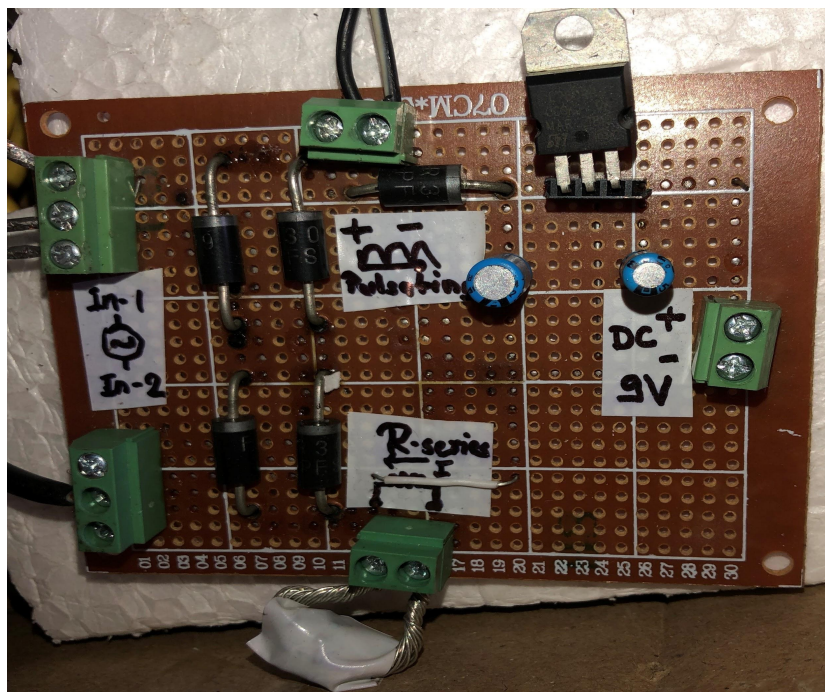


Fig 4.27: Voltage Controlled Oscillator Schematic

The voltage-controlled oscillator is the oscillator that produces square wave signals with variable frequency. The frequency of this oscillator can be controlled by

voltage. UA741 op-amp is used as an inverting amplifier that inputs a signal of 0 to 5 V and mapped it into 4.5 to 5V. The preset on the op-amp side is used to adjust or tune the parameters of the non-inverting amplifier. The output from the op-amp which is 4.5 to 5 is given to the gate side of optocoupler PC817 with a series preset to adjust the gain. Two optocouplers are connected in such a way that the current on the output side can flow bidirectionally. Combinedly these two optocouplers act as voltage-controlled resistance. This resistance is in series with the diode and capacitor as in the schematic. The diodes are Schottky since it involves high frequency. Two diodes in opposite directions are to make an output rectangular wave of 50% duty cycle. A change in resistance changes the frequency of the output square wave of the NE555 timer in astable mode. So finally voltage can control the frequency of the output of the NE555 timer. The output is given to the gate driver. The voltage-controlled oscillator is used for maximum power tracking. All the circuits are fabricated on matrix boards.

#### 4.2.11 Output Rectifier and Voltage Regulator



**Fig 4.28: Output Rectifier and Voltage Regulator Hardware**

The output rectifier consists of a bridge rectifier with four Schottky diodes of rating 3A. The reason behind the use of Schottky diodes is for high-frequency purposes. The load is connected after the rectification. The output is high-frequency pulsating DC. There is also a half-bridge rectifier whose output is fed to the 9V voltage regulator. This regulator is used to supply power to the electronics of the receiver circuit.

## CHAPTER FIVE

### RESULTS AND DISCUSSION

After completing the preparation of the hardware prototype, the system was then tested. Various parameters like frequency, load, and coil distance were varied to collect the data. Two major steps were performed after the gathering of the data:

1. Observation of waveforms
2. Collection and interpretation of the data

#### 5.1 Observation of Waveforms

The waveforms of the systems at various stages were then observed and compared with the simulated waveforms. The waveforms of the following were observed:

1. Gate driving transformer outputs
2. The output of the Inverter
3. Receiver output
4. Receiver output when using LED lights as load

##### 5.1.1 Gate Driving Transformer Outputs

The output of the gate driving transfer which controls the gating signal of the inverter was observed in Fig 5.1.

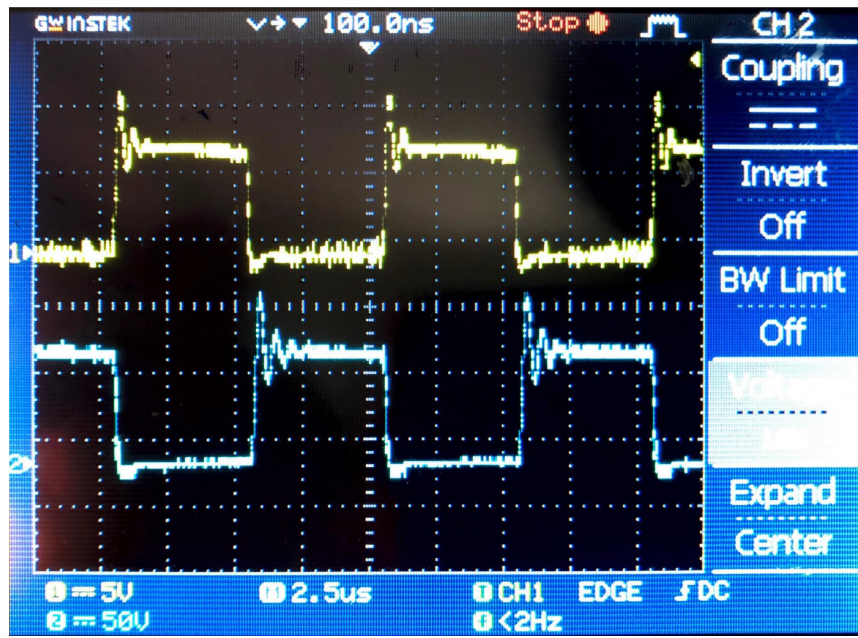


**Fig 5.1: The Output of the Gate Driving Circuit**

As we can see, two completely out-of-phase square wave signals were generated from the gate driving circuit. The small number of harmonics can be seen in the waveform which is found to cause a small amount of loss without affecting the gating sequence.

### 5.1.2 Output of the Inverter

The output of the inverter was then observed. As the gating signals were tested, the output of the inverter was expected as a square wave. However, the output was found to be not a perfect square wave, because of the resistance offered by the MOSFET causing some voltage drop across it.

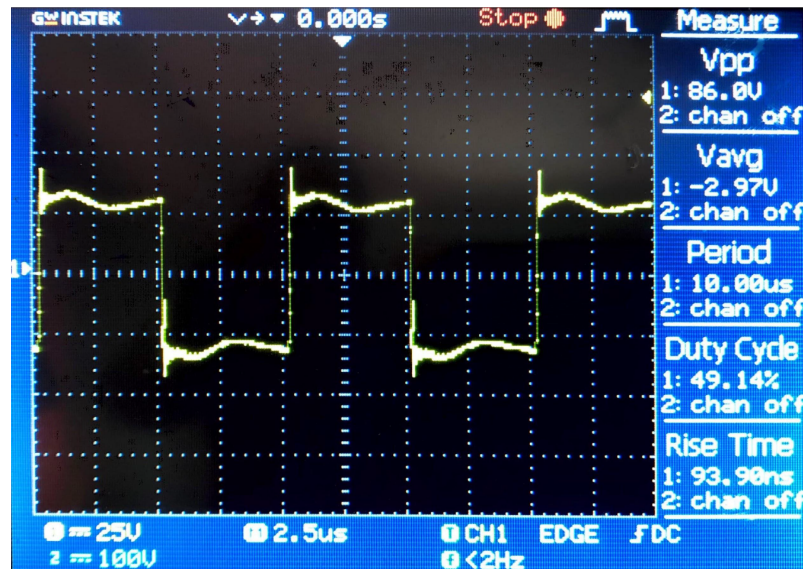


Fig 5.2: Inverter Output Signal

### 5.1.3 Receiver Output

Finally, the output waveform is then observed using the resistors as a load (which is used for all loading conditions to collect the data). As expected, the output voltage wave is perfectly sinusoidal with different magnitudes depending upon varying conditions.

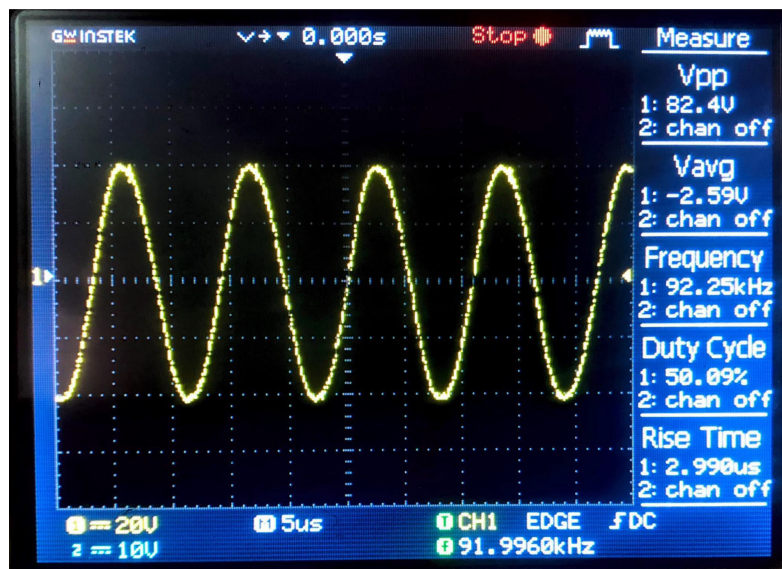


Fig 5.3: Output Signal at Receiver Side with Resistive Load

#### 5.1.4 Receiver Output when using LED Lights as the Load

For a demonstration of the power transfer of the system, LED lights were connected to the receiver as the load. As it is not a linear load, the voltage at the output of the receiver is not sinusoidal. This is due to the impedance offered by the leakage reactance and the compensating capacitor with a non-linear load at the end.



Fig 5.4: Output Signal at Receiver Side with LED Load

After observing the waveforms, and verifying them with expected waveforms, the data were then collected.

#### 5.2 Collection and Interpretation of the Data

The effect of variation in frequency, distance, and load was then studied after the collection of data on these variations. As we have three independent parameters to be varied, each parameter was varied independently after the completion of another variation. We varied the frequency from 92 to 100kHz at steps of 1kHz. The distances varied from 10cm, 15cm, and 20cm. As each resistor of 20 ohms was used, we varied the load from 8 of them in parallel to no-load condition by adding or removing 2 of them at a time.

The following plots are made after data collection:

1.  $P_{out}$  vs f and  $V_{out}$  vs f for  $R_L = 20/6$  ohm at different distances
2.  $P_{out}$  vs f and  $V_{out}$  vs f for  $R_L = 20/4$  ohm at different distances
3.  $P_{out}$  vs f and  $V_{out}$  vs f for  $R_L = 20/2$  ohm at different distances
4. Efficiency vs load for the open circuit at different distances

### 5.2.1 $P_{out}$ vs f and $V_{out}$ vs f for $R_L = 20/6$ Ohm at Different Distances

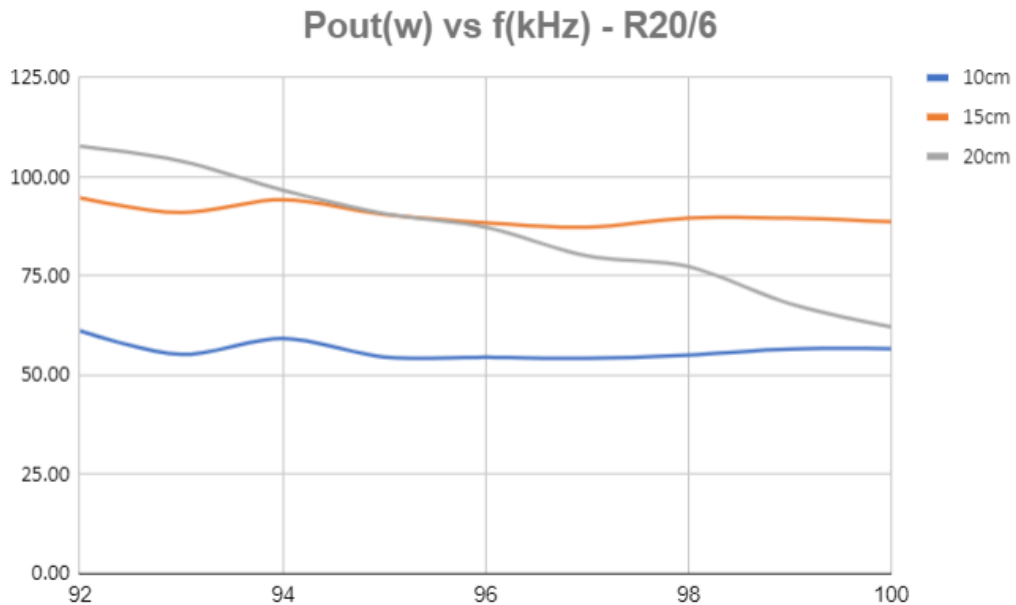


**Fig 5.5:  $P_{out}$  vs f at 20/6 Ohm**

The output power remains almost constant with frequency variation in case of separation of 10cm and 15cm but the output power decreases with an increase in frequency for separation of 20cm.

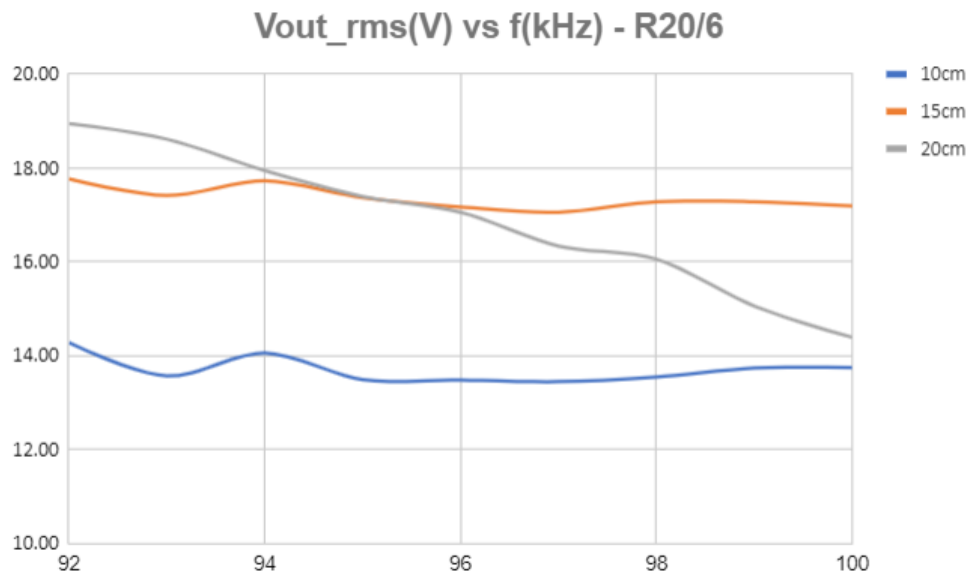


**Fig 5.6:  $V_{out}$  vs f at 20/6 Ohm**

The output voltage remains almost constant with frequency variation in case of separation of 10cm and 15cm but the output power decreases with an increase in frequency for separation of 20cm.

### 5.2.2 $P_{out}$ vs f and $V_{out}$ vs f for $R_L = 20/4$ Ohm at Different Distances

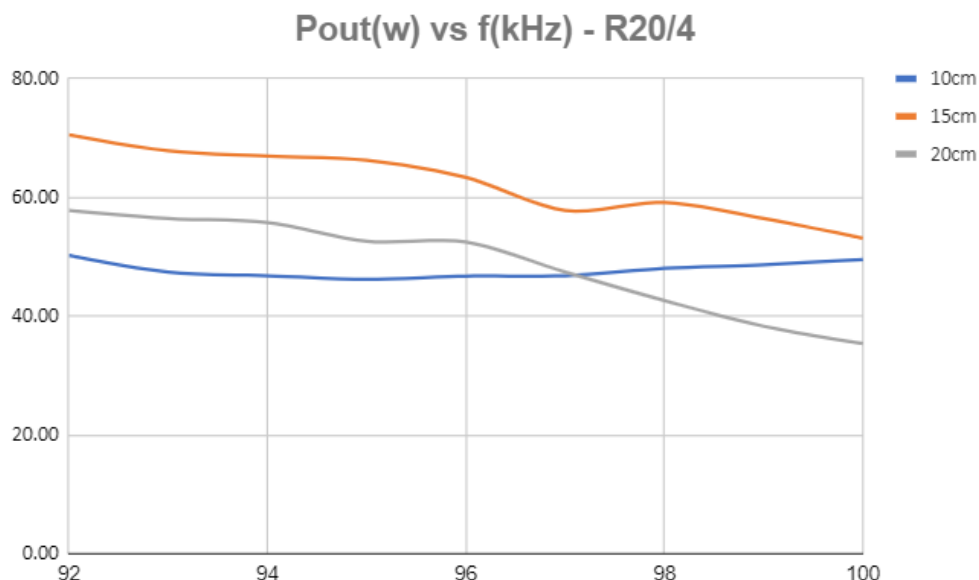


**Fig 5.7:  $P_{out}$  vs f at 20/4 Ohm**

The output power for 15cm and 20cm seems to decrease as the frequency increases, however for the 10cm distance, the power decreases at first and then again increases as frequency increases.

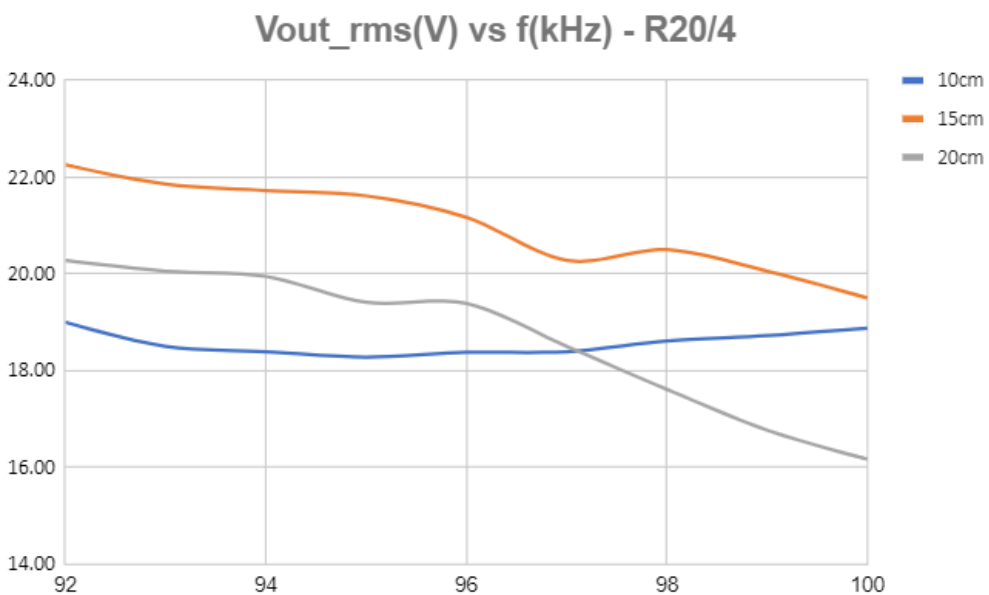


**Fig 5.8:  $V_{out}$  vs f at 20/4 Ohm**

The voltage for this load follows the same nature as for the power but the voltage decreases more rapidly at the distance of 20cm.

### 5.2.3 $P_{out}$ vs f and $V_{out}$ vs f for $R_L = 20/2$ Ohm at Different Distances

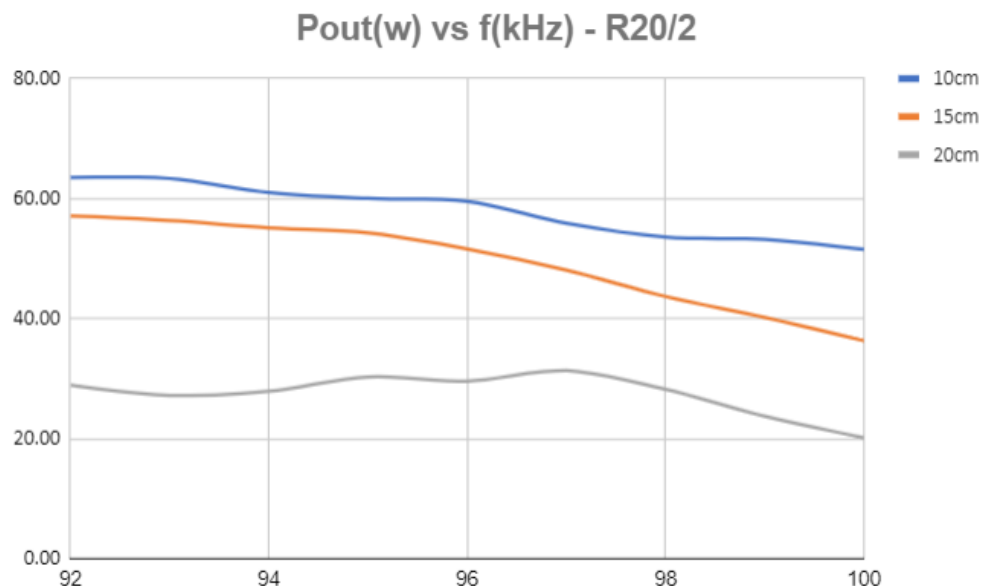


**Fig 5.9:  $P_{out}$  vs f at 20/2 Ohm**

The output power decreases with an increase in frequency for all the distance values but the decrease in power is more rapid for 20cm distance in comparison to the other two values.

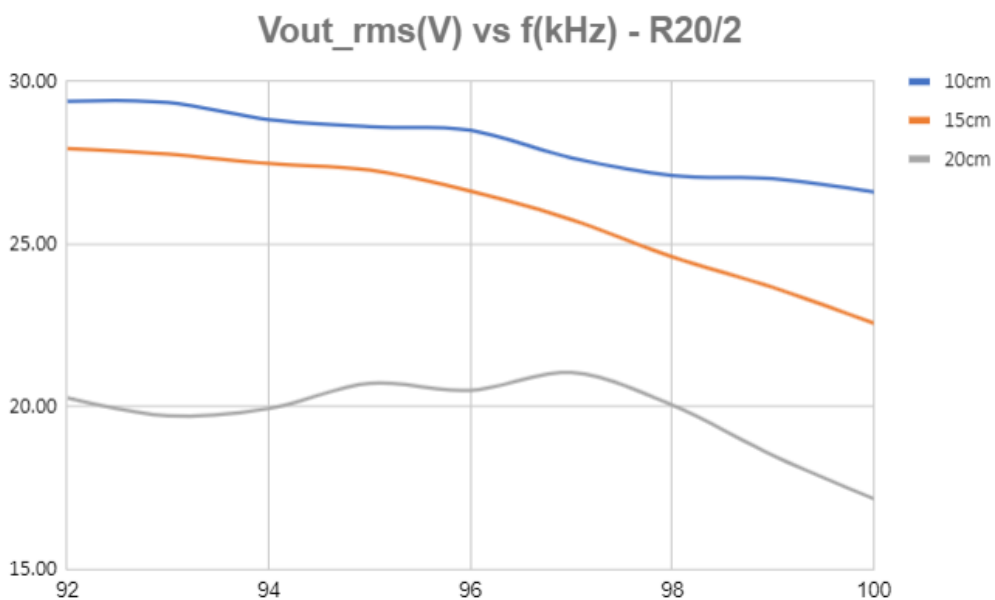


**Fig 5.10:  $V_{out}$  vs f at 20/2 Ohm**

The voltage curves follow the same nature as that of the power.

#### 5.2.4 Max Efficiency vs Load for the Open Circuit at Different Distances

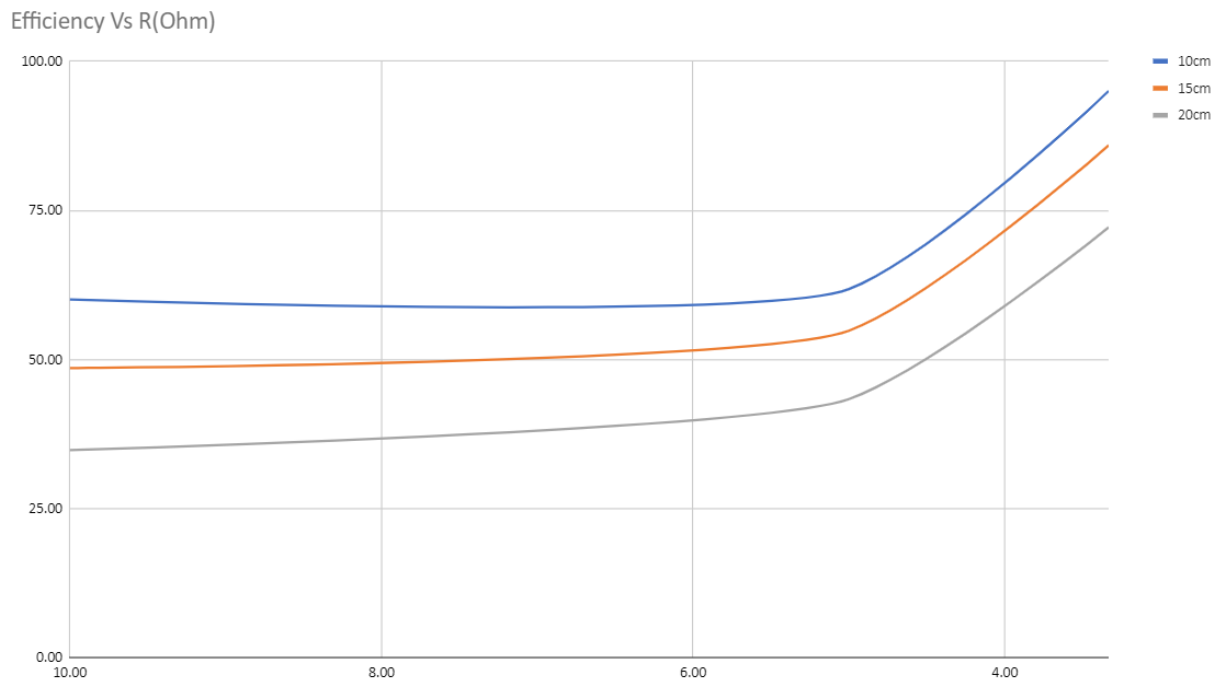


**Fig 5.11: Max Efficiency vs Load**

This plot shows the variation of maximum efficiency with the load. The value of maximum efficiency first remains constant up to a certain value and then starts increasing monotonously as the load increases.

As the load increases, the efficiency curve stretches towards high-efficiency values for all the distance values. As the efficiency can't be increased beyond a certain point because of the constant losses, at very high values of loads, efficiency becomes equal for any distance. Therefore distance doesn't affect efficiency at such low values of load. But at a lighter load, increasing the separation lowers the efficiency. At load values below a certain point, maximum efficiency remains almost constant and is affected by the distance parameters. That load can be termed the critical load. Therefore, the efficiency can be made independent of distance at very high values of loads.

## **CHAPTER SIX**

### **CONCLUSION AND RECOMMENDATION**

Magnetic Resonance WPT can be used to provide autonomous and safer charging options for Electric Vehicles. They can certainly reduce the hassle due to wires and the danger of electrocution to operators even while maintaining high efficiency. We were able to transfer 100W power to a distance of 10cm at a frequency of 100kHz. We had originally planned to be able to completely charge an electric scooter by transferring 1.1 kW power at a distance of 20cm at 85kHz all while maintaining high efficiency, high power factor, and minimum total harmonic distortion. We had to drop the power factor correction circuit and harmonics inhibitor due to limitations of the capital and the costs available for the project implementation in the hardware. We have however prepared simulations for such implementation. The setup had to be redesigned for transferring lower powers at reduced voltage also because ferrite cores for high frequency were not easily available. To conclude, we were able to successfully transfer power wirelessly using Inductive power transfer in resonance conditions. The effect of distance on efficiency decreased as the load increased, and even better results could be achieved had it been designed for a higher power.

In the future with the use of the core, we can transfer 1kW or more than 1kW of power at the same distance. Using the frequency sweeping can be used to track maximum power points. It might prove to be useful against misalignments and variable distance problems for some ranges. Shielding can be improved with the use of cores. Also, efficiency can be improved by using GAN MOSFETs to produce pure sine waves as the output of the inverter instead of square waves.

## REFERENCES

- [1] [https://en.wikipedia.org/wiki/Wireless\\_power\\_transfer](https://en.wikipedia.org/wiki/Wireless_power_transfer)
- [2] Triviño-Cabrera, A., González-González, J. M., & Aguado, J. A. (2020). Wireless power transfer for electric vehicles: foundations and design approach (p. 175). Berlin: Springer.
- [3] Shinohara, N. (Ed.). (2018). Wireless power transfer: theory, technology, and applications (Vol. 112). Energy Engineering.
- [4] Imura, T. (2020). Wireless Power Transfer: Using Magnetic and Electric Resonance Coupling Techniques. Springer Nature.
- [5] Rim, C. T., & Mi, C. (2017). Wireless power transfer for electric vehicles and mobile devices. John Wiley & Sons.
- [6] <https://www.elprocus.com/what-is-half-bridge-inverter-circuit-diagram-its-working/>
- [7] <https://www.elprocus.com/what-is-half-bridge-inverter-circuit-diagram-its-working/>
- [8] <https://electricalworkbook.com/single-phase-half-bridge-inverter/>
- [9] Timilsina, A., Nepali, B., Paudyal, B., Kunwar, J. D., Mishra, A. K., Tamrakar, I., & Ghimire, S. K. A Novel Approach for Wireless Power Transfer Using Magnetic Resonant Method.
- [10] El-Shahat, A., Ayisire, E., Wu, Y., Rahman, M., & Nelms, D. (2019). Electric vehicles wireless power transfer state-of-the-art. *Energy Procedia*, 162, 24-37.
- [11] Asa, E., Pries, J., Galigekere, V., Mukherjee, S., Onar, O. C., Su, G. J., & Ozpineci, B. (2020, March). A novel AC to AC wireless power transfer system for EV charging applications. In 2020 IEEE Applied Power Electronics Conference and Exposition (APEC) (pp. 1685-1690). IEEE.
- [12] Pellitteri, F., Boscaino, V., Di Tommaso, A. O., Miceli, R., & Capponi, G. (2013, October). Wireless battery charging: E-bike application. In 2013 International Conference on Renewable Energy Research and Applications (ICRERA) (pp. 247-251). IEEE.
- [13] Kwan, C. H., Arteaga, J. M., Yates, D. C., & Mitcheson, P. D. (2019, June). Design and construction of a 100 w wireless charger for an e-scooter at 6.78 mhz. In 2019 IEEE PELS Workshop on Emerging Technologies: Wireless Power Transfer (WoW) (pp. 186-190). IEEE.
- [14] Miller, J. M., Onar, O. C., & Chinthavali, M. (2014). Primary-side power flow control of wireless power transfer for electric vehicle charging. *IEEE journal of Emerging and selected topics in power electronics*, 3(1), 147-162.

- [15] Thrimawithana, D. J., & Madawala, U. K. (2010, March). A primary side controller for inductive power transfer systems. In 2010 IEEE International Conference on Industrial Technology (pp. 661-666). IEEE.
- [16] Bosshard, R., Kolar, J. W., Mühlethaler, J., Stevanović, I., Wunsch, B., & Canales, F. (2014). Modeling and  $\eta$ - $\alpha$ -Pareto Optimization of Inductive Power Transfer Coils for Electric Vehicles. IEEE Journal of Emerging and Selected Topics in Power Electronics, 3(1), 50-64.